PACIFIC EARTHQUAKE ENGINEERING
RESEARCH CENTER

Experimental Study of Large Seismic Steel Beam-to-Column Connections

Egor P. Popov
Shakhzod M. Takhirov
Department of Civil Engineering
University of California, Berkeley

PEER 2001/01
NOVEMBER 2002

Experimental Study of Large Seismic Steel Beam-to-Column Connections

Egor P. Popov
Shakhzod M. Takhirov
Department of Civil and Environmental Engineering
University of California, Berkeley

PEER Report 2001/01
Pacific Earthquake Engineering Research Center
College of Engineering
University of California, Berkeley
November 2000

ABSTRACT

Two large bolted steel moment-resisting connections were studied by experiments. These connections were single-sided beam-column assemblies that are representative of exterior beam-column connections. They were composed of W36x150 Grade 50 beams and W14x257 Grade 50 columns. T-sections were cut from W40x264 sections of Grade 50 steel. The T-section webs were welded to the beams and prestressed by bolts to the beam flanges in the shop. Final beam-to-column assembly required no additional welding: the T-section flanges were bolted to the column and the column shear tab was bolted to the beam web. The specimens had two symmetrically located T-sections with different web geometry: Specimen 1 had rectangular-shaped webs, whereas Specimen 2 had U-shaped webs. During cyclic testing beam deformation was minimal due to active participation of the T-section flanges: a separation between T-section flanges and the column flanges was observed. This separation occurred due to bending plastic deformation in the T-section flanges. This phenomenon allowed dissipating energy and prevented severe buckling in the beam flanges and beam web.

ACKNOWLEDGMENTS

This work made use of Pacific Earthquake Engineering Research Center Shared Facilities supported by the Earthquake Engineering Research Center Program of the National Science Foundation under Award Number EEC-9701568.

Many individuals contributed to this research. Partial financial support by Professor Armen Der Kiureghian of the University of California, Berkeley, for the successful completion of the project is greatly appreciated. Thanks are also due to Lev Stepanov of UC Berkeley for his help with high-strength bolt testing and to Don Clyde of PEER for his assistance with the tests.

CONTENTS

LIST OF FIGURES

LIST OF TABLES

1 Review of the Previous Research

1.1 INTRODUCTION

The generally accepted detail of attaching steel beams to columns in seismic applications consists of shear tabs attached to the column and direct welding of beam flanges with cover plates to column flanges. Numerous tests of this type of a connection were supported by the National Science Foundation (NSF), with many specimens donated by the fabricators. The testing of such specimens was organized by the SAC Joint Venture.

The moment capacity of such connections depends on the cyclic endurance of the flange welds in both tension and compression. Under these conditions numerous tension weld failures were observed both in the laboratory and the field. Therefore, it appears to be advantageous to use high quality bolts in tension and to take advantage of shop fillet welds in other details.

1.2 OVERVIEW

The above approach was tried on several end-plate connections by K. C. Tsai and E. P. Popov at the University of California, Berkeley (1988 and 1990). An example of this kind of connection is shown in Figure 1-1. It is of interest to note that direct welding of a beam to a column stub (Specimen 9) results in good behavior, but the fabrication is not generally practical. Specimen 10 with no ribs over the beam flanges did not give satisfactory results. Specimen 10R with ribs over the beam flanges at the column stub behaved very well under cyclic loading, as can be seen in Figure 1-2. Note the required large thickness of the end plate.

The above approach was also pursued recently by T. M. Murray and his at Virginia Polytechnic Institute (VPI) with good results. They achieved a number of successful tests with W36x150 beams. It appears that for larger or heavier beams the use of ribs over beam flanges at columns would be required.

An extensive excellent study of bolted connections was done last year at Georgia Institute of Technology by R. Leon and his associates. The work is very comprehensive but is limited to small- and medium-size members.

The newly developed and tested connection at the University of California, Berkeley, is somewhat related to the end plate connection but is more versatile as it is more readily

adaptable to a larger range of heavier beams. The new connection depends on the use of A490 1-¼ ″ bolts in tension in oversize round holes and shop fillet welds.

1.3 TENSION TESTS ON A490 1-¼″ BOLTS

In order to conduct a ductility study on the A490 1-¼″ bolts two tests were performed. For the first test, a special device was built to test simultaneously the shank of the bolt and the threaded part of the bolt below the nut. The actual failure occurred in the threaded region. The remarkable ductility of the A490 bolt was clearly demonstrated; the load versus elongation diagram is presented in Figure 1-3. Another experiment on a specimen of constant diameter machined from a A490 bolt also showed excellent ductility. Figure 1-4 shows the stress-strain diagram for this test.

1.4 TEST SPECIMEN DESIGN AND DETAILING

One newly developed connection using A490 1-¼″ bolts is shown in Figure 1-5. The details for the two specimens are shown in Figures 1-6 and 1-7. In both cases the attachment of a beam to a column is made using structural T's cut from W shapes (T-sections). A large choice of such sections is available. By rotating the beam all fillet welds can be done in the shop in a down-hand position. Generous rounded fillets occur in all cases between a flange and the stem of the T-sections. Shop experience in fabricating these two specimens was very encouraging.

The maximum beam moment for this type of connection was calculated as follows. According to FEMA 267A, *Interim Guidelines* (FEMA 1995b) the maximum beam moment, M_{pr}, at the plastic hinge is equal to $1.1Z_bF_y$, where Z_b is the plastic section modulus at the plastic hinge that was assumed to form at $d_b/4$ beyond the web of the T-section, where d_b is the depth of the beam. The moment at the column face is M_{col}. For each specimen M_{pr} =*35,100 kip-inch*, M_{col} =*45,500 kip-inch*.

.

2 Experimental Program

2.1 INTRODUCTION

This section summarizes the results of cyclic testing of two full-scale beam-column bolted connection specimens. The specimens were designed by Popov and were fabricated by Stoltz Metals, Inc. The tests were carried out in the Structural Research Laboratory of the Pacific Earthquake Engineering Research Center, University of California, Berkeley. The tests were conducted under gift funding. The Principal Investigator was Professor Armen Der Kiureghian.

2.2 TEST SPECIMENS, TEST SETUP, AND INSTRUMENTATION

2.2.1 Test Specimens

The beams were fabricated from W36x150 sections of A572-Gr.50 steel, the columns were fabricated from W14x257 sections of A572-Gr.50 steel. The T-sections were made from W40x264 sections of A572-Gr.50 steel. The global dimensions and geometry of the specimens are shown in Figure 1-5. Figures 1-6 and 1-7 show the design details for Specimen 1 and Specimen 2. The material properties of the connections from mill certificate data are presented in Table 2-1. The specimens had two symmetrically located T-sections with different in web geometry: Specimen 1 had rectangular webs, whereas Specimen 2 had U-shaped webs. The T-sections were welded to the beams in the shop, and were later bolted to the columns.

2.2.2 Test Setup

The specimens were tested in the Structural Research Laboratory of PEER, UC Berkeley. The test setup was designed to accommodate specimens with columns in a vertical position, as shown in Figure 2-1. The specimens were attached to two steel frames: a horizontal one and a vertical reaction one. The horizontal steel frame was prestressed to the strong floor. The columns in the test specimens were attached to the horizontal frame and the vertical reaction frame using short segments of W14x311 to achieve near pinned boundary conditions.

The load was applied to the cantilever beam end by a 400-kip (1,800-kN) hydraulic actuator, through a clevis bolted to the beam end plate. The testing setup had a

displacement capacity of ±7.75 in. (197 mm) and a load capacity of ±350-kip (1,575-kN). No axial load was applied to the column. The test was conducted using the beam end displacement control. The beam end was at a distance of 130 in. (3.3 m) from the column face. To prevent out-of-plane movement of the beam, a vertical bracing system was provided near the beam end. The photograph (Fig. 2-2) shows a view of a test in progress.

2.2.3 Instrumentation

Many sensors were used to monitor the response of the specimens during the test in order to understand the specimen behavior. Figure 2-3 shows the location of displacement measuring instruments on the specimens. The imposed displacement at the end of the beam was measured by a linear variable differential transformer (LVDT). This displacement is denoted by δ, a load cell in-line with the actuator-measured axial force P. The direct current differential transformers (DCDTs) were used to provide the remaining displacement measurements. The deformation of the beam panel zone was calculated from readings at δ_1 and δ_2 DCDT locations. The global deflection shape of the column was measured by δ_3 – δ_6 displacement transducers. The amplitude of the gap opening between the T-section flanges and the column flanges was measured by two displacement transducers, δ_7 and δ_8.

Strain gages and rosettes were glued at critical locations to investigate local response. Figures 2-4 and 2-5 show these locations on Specimen 1 and Specimen 2, respectively. Thirty-eight channels of data were used during testing. Tables 2-2 and 2-3 present information on the instrumentation with the channel number, name of the measuring device, and the device location.

2.2.4 Data Acquisition

The test control and the data acquisition system were run by a Windows-based control and acquisition program called Automated Testing System (ATS) developed by SHRP Equipment Corporation of Walnut Creek, California. This program is capable of signal generation, four-channel servo-actuator command, and 16-channel data acquisition. For the tests the ATS system was used to monitor and control the displacement and force-feedback signals.

Other data were monitored and recorded using an AutoNet data acquisition system with a capacity of 64 channels. Pacific Signal Conditioners were used to amplify the transducers and the strain gages signals and to remove frequencies above 100 Hz from the analog signal.

2.2.5 Loading History

The testing program was based on the ATC-24 document *Guidelines for Cyclic Seismic Testing of Components of Steel Structures.* The specimens were tested under displacement control, following a loading history consisting of stepwise increasing deformation cycles. At a certain stage of plastic deformation of the specimens, cycles with small amplitudes were imposed. Each loading step was defined by the peak beam end displacement and by the number of cycle. Table 2-4 presents the testing program for Specimens 1 and 2.

2.2.6 Data Processing

Specimen behavior was characterized by the following parameters: applied load, beam end displacement, total plastic rotation of the connection, panel zone shear deformation, column deformation, deformation in the T-section flange, and beam deflection. A test specimen layout, the corresponding measurements, the chosen positive direction of the applied load, and the measured displacements are shown in Figure 2-3.

The total displacement of the beam end, δ_{total} , is caused by the rigid body motion of the connection, the deformations of the beam itself, the column, the panel zone, and deformation in the T-section flange. The rigid body motion was possible due to the small flexibility of the vertical reaction frame. This part of the displacement was not large but could not be neglected. Therefore the beam end relative displacement δ was calculated from the total one by subtracting the rigid body displacement. As a result of the column and panel zone deformations, the panel zone rotates through an angle, θ_c, and changes its initial configuration. Four displacement measurements (δ_1, δ_2, δ_4, and δ_5) were used to compute the connection rotation due column deflection, θ_c, and panel shear deformation, γ. The total beam rotation, θ, can be separated into four components: rotation due to deformation of the beam itself, θ_b; rotation caused by rigid connection rotation, θ_c; the contribution from the panel zone, γ, and the rotation due to the gap opening in the T-sections, θ_T. These values were determined as follows:

- Total beam end displacement: $\delta_{total.}$
- Relative beam end displacement: $\delta = \delta_{total} - L\,(\delta_6 - \delta_3)/H$. The rest of the calculation was done using this value of the displacement; where H is a distance from pin to pin, and L is the distance from the beam end to the center line of the column.
- Total rotation: $\theta = \delta / L$.
- Connection rotation due to column deflection: $\theta_c = (\delta_5 - \delta_4)/d$, where d is a distance between continuity plates.
- Panel zone shear deformation: $\gamma = (\delta_5 - \delta_4)\sqrt{a^2 + b^2}/(2ab)$, where a and b are the dimensions of the rectangular panel zone area (distance between targets in the horizontal and vertical directions).

- Rotation due to the gap opening (and deformation) between the T-section flange and the column flange: $\theta_T = (\delta_8 - \delta_7)/d$.
- Total plastic rotation: $\theta_{pl} = \theta - M/K_\theta$. Where $M = PL_0$ (L_0 is a distance from center-line of the actuator to the face of the column) is the moment at the face of the column and K_θ is the elastic stiffness determined from M versus θ_{pl} curve. The unloading path of one of the elastic cycles below the reverse point was used to estimate this stiffness, to avoid the influence of initial imperfections, clearances, hysteresis, etc.

A set of programs for the MATLAB 5.3 environment was created to process data and to plot results in accordance with the procedure described above.

2.3 TEST RESULTS

2.3.1 Specimen 1

Testing of the first specimen was conducted on July 30, 2000. The specimen sustained all loading steps up to and including the 5.69″ beam tip displacement cycles without significant damage. Testing was stopped because the maximum load for the test setup was reached. A close-up side view of the specimen after the test is presented in Figure 2-6. During the last set of the load reversals a light buckling in the beam web and flanges was observed. The residual buckling in the beam flange and web is shown in Figures 2-7 and 2-8. During the test energy was dissipated by cyclic yielding of the flanges of the T-sections, and the gap between the T-section and column flanges opened and closed periodically. The residual gap in the upper T-section is shown in Figure 2-9.

Table 2-4 presents the loading protocol for Specimen 1. The loading history is plotted in Figure 2-10.

The plot of the applied force versus beam tip displacement response, δ_{total}, is presented in Figure 2-11. The values of the displacement were obtained directly from the LVDT reading. The relative displacement, δ, was calculated from the previous displacement by subtracting the specimen's displacement as a rigid body. Because some small flexibility occurred in the vertical reaction frame, this displacement could not be neglected. The plot of the applied force versus relative beam tip displacement is presented in Figure 2-12.

The total beam rotation is calculated based on the values of the relative beam tip displacement. The imposed moment versus beam total rotation is presented in Figure 2-13. Figure 2-14 shows the applied moment versus the beam plastic rotation. The deformation of the column panel zone is presented in Figure 2-15.

During the test the visible opening between the T-section flanges and the column flanges was observed. The amplitudes of the gap opening at the flanges were measured by DCDT. Figures 2-16a and 2-16b show these values during the test. The gap opening between the T-section flange and the column flange for the upper T-section is presented

in Figure-16a. The same value for the lower T-section is presented in Figure 2-16b. The beam rotation due to these openings in the T-sections are presented in Figure 2-17.

The imposed force versus beam rotation due to the panel zone rotation is presented in Figure 2-18. The relative beam rotation calculated by subtracting the rotation of the panel zone, the rotation due to gap opening in the T-sections, and the panel zone deformation are presented in Figure 2-19.

The local strain changes during the test are given in Figures 2-20, 2-21, and 2-22. Figure 2-20 shows the local strain in the middle of the top flange (gage SG2) near the web end of the T-section. Figure 2-21 shows the local strain in the T-section's web near the K-line and the location of the external bolt (SG4), whereas Figure 2-22 presents the local strain in the same web in its middle (SG5).

The strain gage data are presented in the following way. Two phases of the testing were chosen: (1) a completely elastic stage (at 1.07″ cycle) and (2) the stage when the specimen had plastic deformations with no buckling (at 2.85″ cycle). The maximum values of the corresponding strains during the chosen cycles were selected and normalized by the maximum strain value. For instance, during the first stage the maximum value of the strain was obtained at the location of the strain gage, SG5, and was 0.20%. The strain gage readings presented in Figure 2-23 are the fraction of the obtained values to 0.20%. During the cycles with 2.85″ beam tip displacement the maximum value was obtained at the location of the strain gage, SG1, and was equal to 0.70%. The strain gage readings for this stage are presented in Figure 2-24. The reading of the strain gage, SG10, is not given here, because the reading was inaccurate.

2.3.2 Specimen 2

Testing of the second specimen was conducted on July 20, 2000. The specimen sustained all loading steps up to the 5.69″ beam tip displacement cycles and failed at the first ramp of the last cycle. The fracture was caused by cracking in the web of the lower T-section. The crack line started at the end of the weld and went through the hole for the 1″ bolt. Testing was stopped after the finish of this cycle. A side view of the specimen after the testing is presented in Figure 2-25.

At the end of the test a light buckle in the beam web and flanges was observed. The residual buckling in the beam flanges is shown in Figures 2-26 and 2-27.

During the test some energy was dissipated by cyclic yielding of the T-sections; the gap between the T-section and the column flanges opened and closed periodically. The residual gap in the top T-section is shown in Figure 2-28.

The crack in the web of the bottom T-section is shown in Figures 2-29 and 2-30. Figure 2-29 shows the location of this crack on the web of the T-section, close to the K-line of the T-section and parallel to it. The crack started from the end of the fillet weld,

continued through the nearest hole for the 1″ bolt, and ended at the next bolt hole. A closeup of the crack is presented in Figure 2-30. The arrows trace the crack.

Table 2-4 presents the loading protocol for Specimen 2. The loading history is plotted in Figure 2-31.

The layout of the displacement measuring instrumentation was identical for both specimens, shown in Figure 2-3. The displacement at the beam tip was measured by LVDT, whereas the remainder of displacement measurement was done using DCDT.

The location of the strain gages is presented in Figure 2-5. This layout was almost the same for both tested specimens, with small difference in distances because of different lengths of the T-section webs.

The plot of applied force versus beam tip displacement is presented in Figure 2-32. The values of the displacements were obtained directly from the LVDT reading. The relative displacement was calculated from the previous displacement by subtracting the specimen's displacement as a rigid body. The flexibility of the reacting frame was taken into account. The plot of applied force versus relative beam tip displacement is presented in Figure 2-33.

The total beam rotation is calculated based on the values of the relative beam tip. The imposed moment versus the beam total rotation is presented in Figure 2-34. Figure 2-35 shows the applied moment versus the beam plastic rotation. The deformation of the column panel zone is presented in Figure 2-36.

During the test a visible opening was observed between the T-section and column flanges. The values of the gap opening were measured by DCDT. Figures 2-37a and 2-37b show these values during the test. The gap opening between the T-section flange and column flange for the top T-section is presented in Figure 2-37a. The same data for the bottom T-section is presented in Fig. 2-37b. The beam rotation due to these openings in the T-sections is presented in Figure 2-38.

The imposed force versus beam rotation due to panel zone rotation is presented in Figure 2-39. The relative beam rotation calculated by subtracting the rotation of the panel zone, the rotation due to gap opening in the T-sections, and the panel zone deformation are presented in Figure 2-40.

The local strain change during the test is presented in Figure 2-41, 2-42, and 2-43. Figure 2-41 shows the local strain near the edge of the lower T-section web, SG 15, where the crack started. The gage reading in the middle of this web, SG14, is presented in Figure 2-42. Figure 2-43 shows the local strain readings in gage SG13; the crack did not reach this gage location during the failure and this part of the web had the high range of plastic deformations. All gage readings are presented up to the moment of failure.

The strain gage data are presented in the same way as for Specimen 1. Two phases of testing were captured: (1) a completely elastic stage (at 1.07″ cycle) and (2) when the specimen had yielding deformations but buckling was not observed at the 2.85″ cycle. The maximum values of the corresponding strains during chosen cycles were selected and normalized by the maximum strain value. For instance, during the first stage, the maximum value of the strain was obtained at the location of the strain gage SG5, and was 0.18%. The strain gage readings presented in Figure 2-44 are the fractions of 0.18%. During the cycles with 2.83″ beam tip displacement the maximum value was obtained at location of the strain gage SG3, and was equal to 1.00%. The strain gage readings for this stage are presented in Figure 2-45.

3 Experimental Results and Conclusions

3.1 EXPERIMENTAL RESULTS

A brief summary of the experimental results and the key parameters characterizing the performance of tested specimens is presented in Table 3-1.

3.2 CONCLUSIONS: ADVANTAGES AND DISADVANTAGES OF PROPOSED CONNECTIONS

3.2.1 Advantages

The design and performance of the proposed beam-to-column connections show the following advantages:

- All welding work can be done in a welding shop, in convenient welding positions.
- Final assembling with bolts is a relatively easy procedure and does not require a rigorous quality assurance inspection. (In order to achieve the required clamping force between the column and the T-section flanges, the widely available torque multiplier from WRIGHTTOOL: Model 9S393A was used; the device does not produce any noise and has an accuracy of ±5%).
- Specimen 2 was disassembled after the test. This procedure showed that repairing and replacing the beam with a new T-section is neither difficult nor expensive.
- Beam deformation is minimal due to active participation of the T-sections flanges and the column flanges during cyclic input.

3.2.2 Disadvantages

The chosen design and the failure of Specimen 2 show the following disadvantages and suggested improvements:

- Steel along the K-line of the T-section must be carefully selected.
- 1″ bolts (as used in Specimen 2 to prestress the T-section web to beam flange) require a greater distance between the bolt and the end of the fillet weld. Alternatively, it appears that the bolts can be omitted altogether.
- Steel material of 1-¼ ″ bolts has to be high quality as used in the tested connections.
- Connections based on the proposed design require shims for field assembly.

References

Applied Technology Council [ATC]. 1992. *ATC-24 Guidelines for cyclic seismic testing of components of steel structures.* Redwood City, Calif.

FEMA. 1995b. *Interim guidelines: Advisory no. 1, supplement to FEMA-267.* FEMA report no. 267. Washington, D.C.: Federal Emergency Management Agency.

Leon, Roberto et al. February 2000. *Tests on bolted connections.* School of Civil and Environmental Engineering, Georgia Institute of Technology. Report No. SEMM 00-02.

Murray, T. M. et al. May 2000. *Cyclic testing of bolted moment end plate connections.* [Blacksburg, Va.]: Structural and Materials Laboratory, Virginia Polytechnic Institute and State University.

Tsai, K. C., and E. P. Popov. 1990. Cyclic behavior of end-plate moment connections. *ASCE J. of Struct. Engineering* 116(11)(November).

Tsai, K. C., and E. P. Popov. 1988. *Steel beam-column joints in moment resisting frames.* Earthquake Engineering Research Center, University of California at Berkeley. Report UCB/EERC 88/19.

Table 2-1. Material properties

No	Part of Connection	Yield Stress [ksi]	Ultimate Stress [ksi]	Section Size	Grade
1	Beam	56.6	74.4	W36x150	Gr50
2	Column	52	66	W14x283	Gr50
3	T-section	64	79	WT40x264	Gr50

Table 2-2. Instrumentation information for Specimen 1

No.	Device*	Measuring response**
1	-	date
2	-	time
3	LC1	actuator force
4	LVDT1	beam end displacement
5	R1-b	beam web, 28.75" from column face, 7" above beam bottom flange,+45 degrees
6	R1-t	beam web, 28.75" from column face, 7" above beam bottom flange,-45 degrees
7	R2-b	beam web, 28.75" from column face, web center line,+45 degrees
8	R2-t	beam web, 28.75" from column face, web center line,-45 degrees
9	R3-b	beam web, 8.25" from column face, 7" above beam bottom flange,+45 degrees
10	R3-t	beam web, 8.25" from column face, 7" above beam bottom flange,-45 degrees
11	R4-b	beam web, 8.25" from column face, web center line,+45 degrees
12	R4-t	beam web, 8.25" from column face, web center line,-45 degrees
13	SG1	beam top flange, 29.75" from column face, 1" from flange edge (north)
14	SG2	beam top flange, 29.75" from column face, flange center line
15	SG3	beam top flange, 29.75" from column face, 1" from flange edge (south)
16	SG4	top cover plate, 4" from column face, 1-5/8" from cover plate edge (north)
17	SG5	top cover plate, 4" from column face, flange center line
18	SG6	top cover plate, 4" from column flange, 1-5/8" from cover plate edge (south)
19	SG7	column face, 25.5" up from column center, 3-3/8" from flange edge (north)
20	SG8	column face, 25.5" up from column center, 3-3/8" from flange edge (south)
21	SG9	center line of top continuity plate , 1" from column interface flange
22	SG10	beam bottom flange, 29.75" from column face, 1" from flange edge (north)
23	SG11	beam bottom flange, 29.75" from column face, flange center line
24	SG12	beam bottom flange, 29.75" from column face, 1" from flange edge (south)
25	SG13	bottom cover plate, 4" from column face, 1-5/8" from cover plate edge (north)
26	SG14	bottom cover plate, 4" from column face, flange center line
27	SG15	bottom cover plate, 4" from column face, 1-5/8" from cover plate edge (south)
28	SG16	column face, 25.5" down from column center, 3-3/8" from flange edge (north)
29	SG17	column face, 25.5" down from column center, 3-3/8" from flange edge (south)
30	SG18	center line of bottom continuity plate , 1" from column interface flange
31	DCDT1	doubler plate diagonal (upward from east-west direction)
32	DCDT2	doubler plate diagonal (downward from east-west direction)
33	DCDT3	level of top I-beam (top pin)
34	DCDT4	level of top continuity plate
35	DCDT5	level of bottom continuity plate
36	DCDT6	level of bottom I-beam (bottom pin)
37	DCDT7	level of top T-section
38	DCDT8	level of bottom T-section

* LC=load cell; LVDT=linear variable differential transformer; R=rosette (shear) gage; SG=uniaxial gage

** See Figure 2-4 for gage locations; ±45 degrees=45 degrees clockwise (ccw) from east-west direction.

Table 2-3. Instrumentation information for Specimen 2

No.	Device*	Measuring response**
1	-	date
2	-	time
3	LC1	actuator force
4	LVDT1	beam end displacement
5	R1-b	beam web, 20" from column face, 7" above beam bottom flange,+45 degrees
6	R1-t	beam web, 20" from column face, 7" above beam bottom flange,-45 degrees
7	R2-b	beam web, 20" from column face, web center line,+45 degrees
8	R2-t	beam web, 20" from column face, web center line,-45 degrees
9	R3-b	beam web, 8.25" from column face, 7" above beam bottom flange,+45 degrees
10	R3-t	beam web, 8.25" from column face, 7" above beam bottom flange,-45 degrees
11	R4-b	beam web, 8.25" from column face, web center line,+45 degrees
12	R4-t	beam web, 8.25" from column face, web center line,-45 degrees
13	SG1	beam top flange, 21" from column face, 1" from flange edge (north)
14	SG2	beam top flange, 21" from column face, flange center line
15	SG3	beam top flange, 21" from column face, 1" from flange edge (south)
16	SG4	top cover plate, 4" from column face, 1-5/8" from cover plate edge (north)
17	SG5	top cover plate, 4" from column face, flange center line
18	SG6	top cover plate, 4" from column flange, 1-5/8" from cover plate edge (south)
19	SG7	column face, 25.5" up from column center, 3-3/8" from flange edge (north)
20	SG8	column face, 25.5" up from column center, 3-3/8" from flange edge (south)
21	SG9	center line of top continuity plate , 1" from column interface flange
22	SG10	beam bottom flange, 21" from column face, 1" from flange edge (north)
23	SG11	beam bottom flange, 21" from column face, flange center line
24	SG12	beam bottom flange, 21" from column face, 1" from flange edge (south)
25	SG13	bottom cover plate, 4" from column face, 1-5/8" from cover plate edge (north)
26	SG14	bottom cover plate, 4" from column face, flange center line
27	SG15	bottom cover plate, 4" from column face, 1-5/8" from cover plate edge (south)
28	SG16	column face, 25.5" down from column center, 3-3/8" from flange edge (north)
29	SG17	column face, 25.5" down from column center, 3-3/8" from flange edge (south)
30	SG18	center line of bottom continuity plate , 1" from column interface flange
31	DCDT1	doubler plate diagonal (upward from east-west direction)
32	DCDT2	doubler plate diagonal (downward from east-west direction)
33	DCDT3	level of top I-beam (top pin)
34	DCDT4	level of top continuity plate
35	DCDT5	level of bottom continuity plate
36	DCDT6	level of bottom I-beam (bottom pin)
37	DCDT7	level of top T-section
38	DCDT8	level of bottom T-section

* LC=load cell; LVDT=linear variable differential transformer; R=rosette (shear) gage; SG=uniaxial gage

** See Figures 2-5 for gage locations; ±45 degrees=45 degrees clockwise (ccw) from east-west direction.

Table 2-4. Testing program for both specimens

Beam end displacement [inch]	0.36	0.53	0.71	1.07	1.42	2.14	0.53	2.85	4.27	5.69
No. of cycles	6	6	6	6	4	2	2	2	3	6*

* Only 2 cycles at this level were performed for Specimen 2.

Table 3-1. Short summary of test results

Key parameters	Specimen 1	Specimen 2
Yield load [kips]	230	230
Beam end displacement at yield point [inch]	1.2	1.1
Elastic stiffness of connection [kips/inch]	180	178
Maximum beam end displacement	5.1	5.1
Beam end displacement at failure [inch]	N/A	3.5
Maximum imposed load [kips]	350	350
Maximum imposed moment [kips*inch]	49000	45000
Maximum connection rotation [rad]	4	4
Maximum plastic connection rotation [rad]	2.5	3.3
Maximum rotation due gap opening [rad]	1	0.7
Maximum relative beam rotation itself [rad]	0.6	1.5*

*This value is high because it includes beam rotation after the bottom beam flange failure.

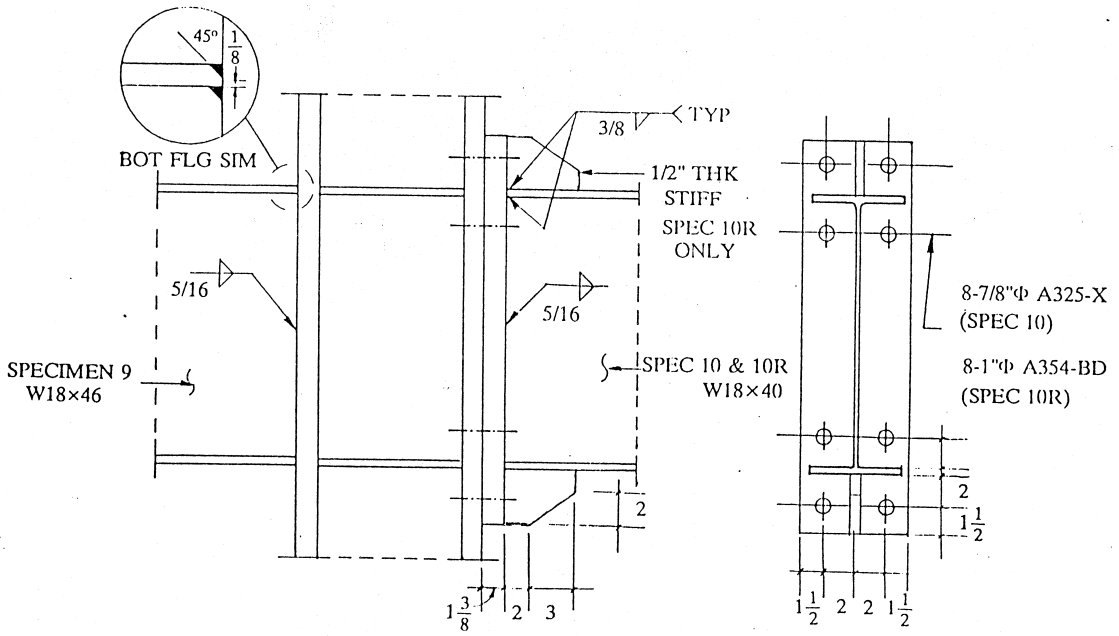

Figure 1-1. Design details of end-plate connections for Specimens 10 and 10R, and that of direct welding to column, Specimen 9 (K. C. Tsai, E. P. Popov 1988, 1990)

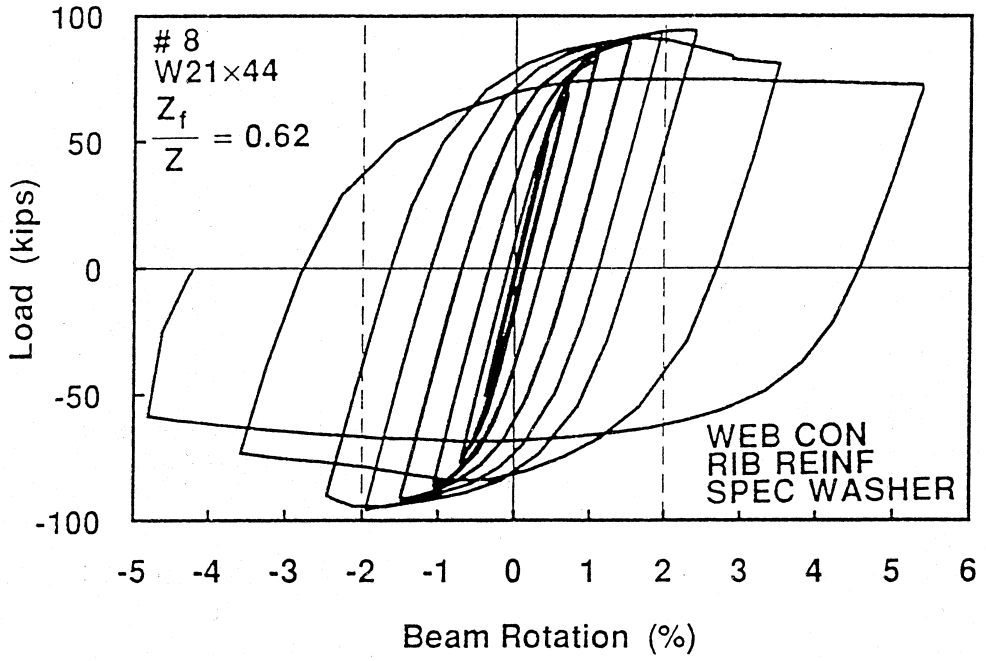

Figure 1-2. Cantilever beam load versus beam rotation for Specimen 10R (K. C. Tsai, E. P. Popov 1988, 1990)

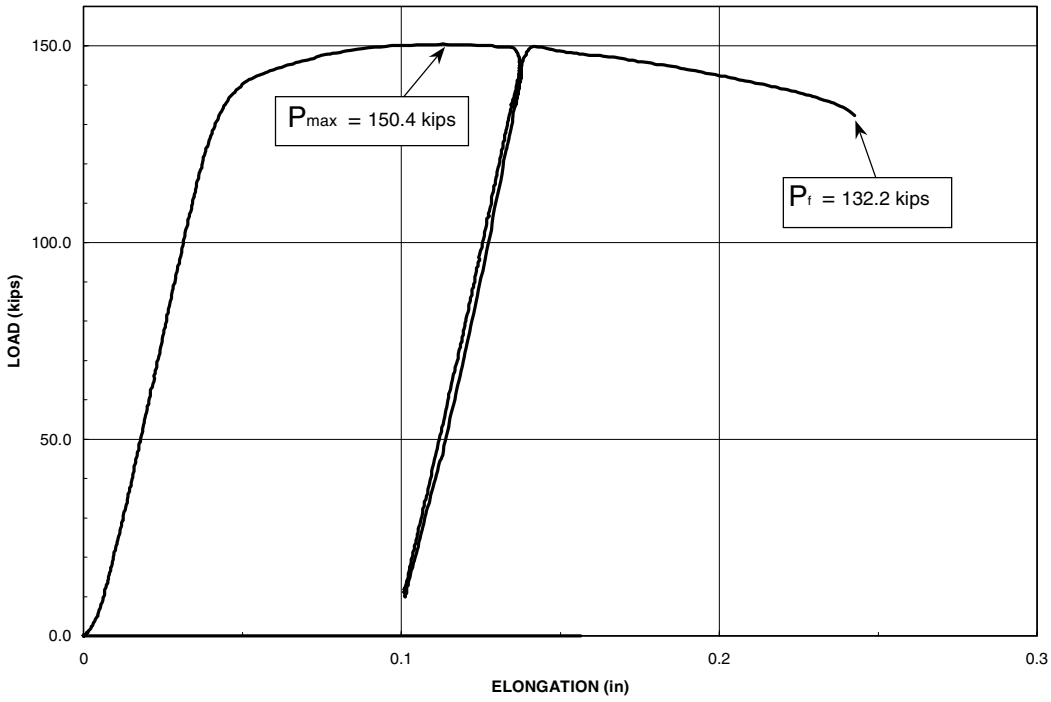

Figure 1-3. Load versus elongation for A490 1-¼″ bolt

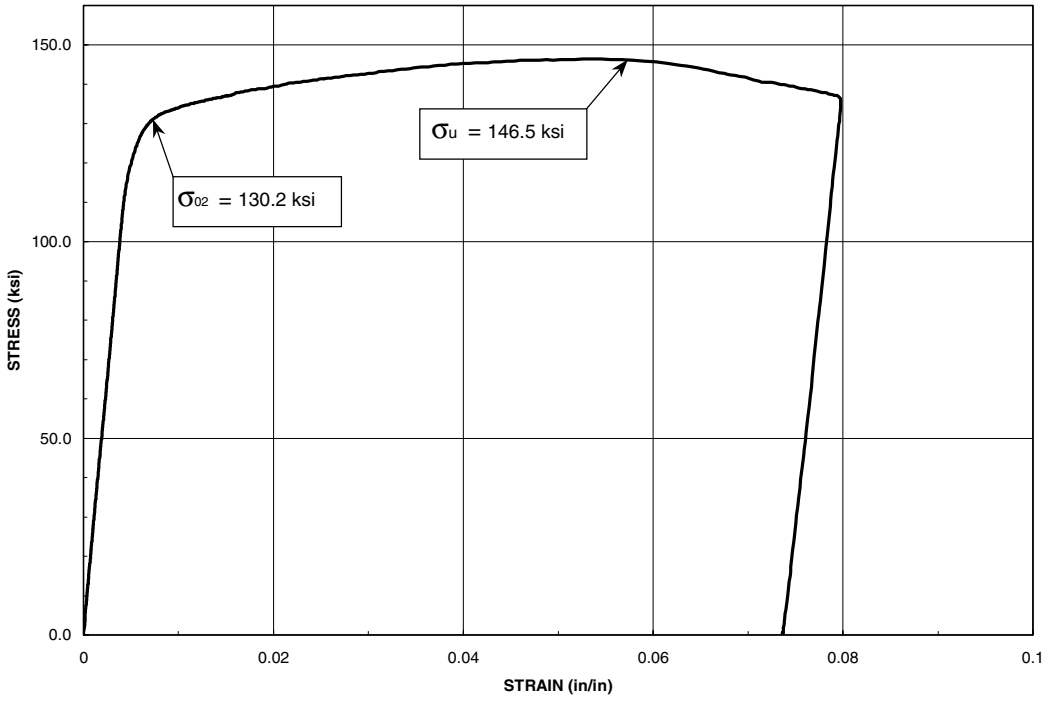

Figure 1-4. Stress versus strain for coupon test of A490 1-¼″ bolt material

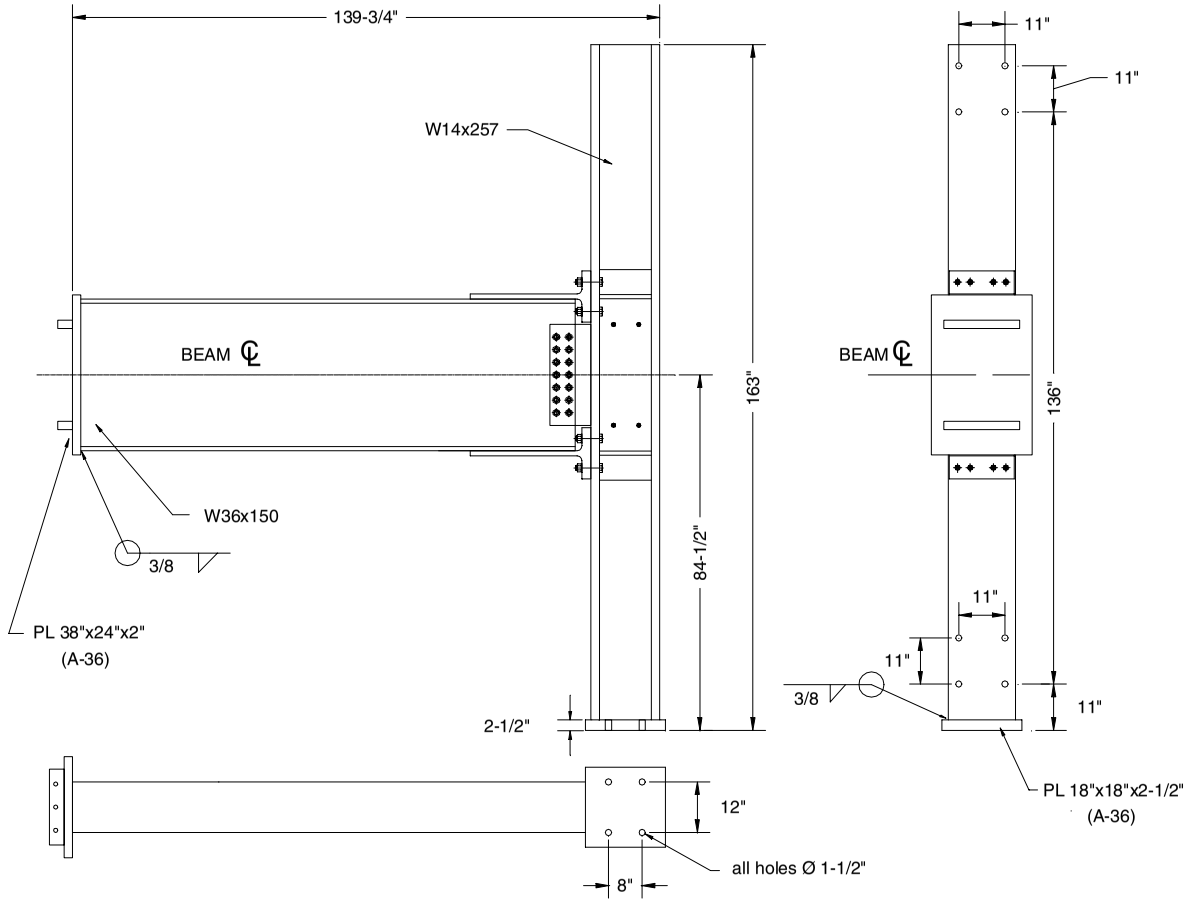

Figure 1-5. Global dimensions and geometry of the tested specimens

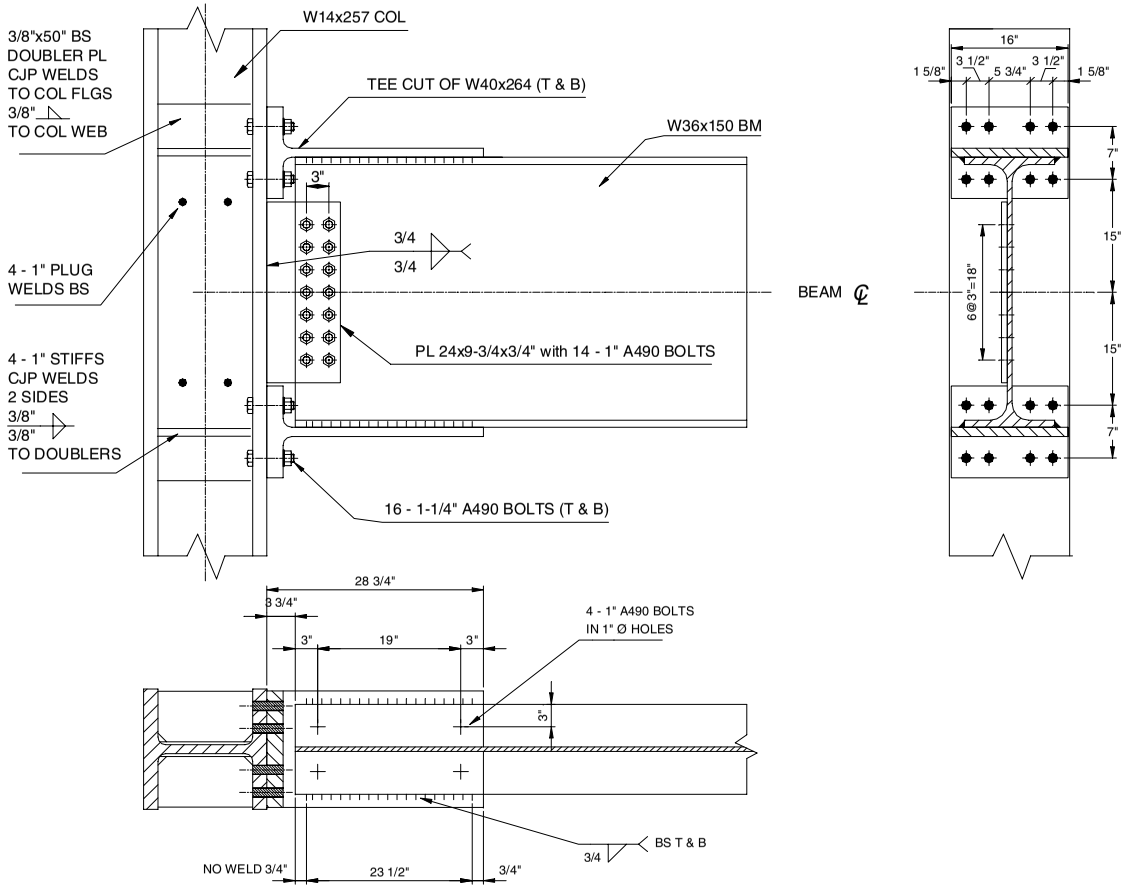

Figure 1-6. Design details of Specimen 1

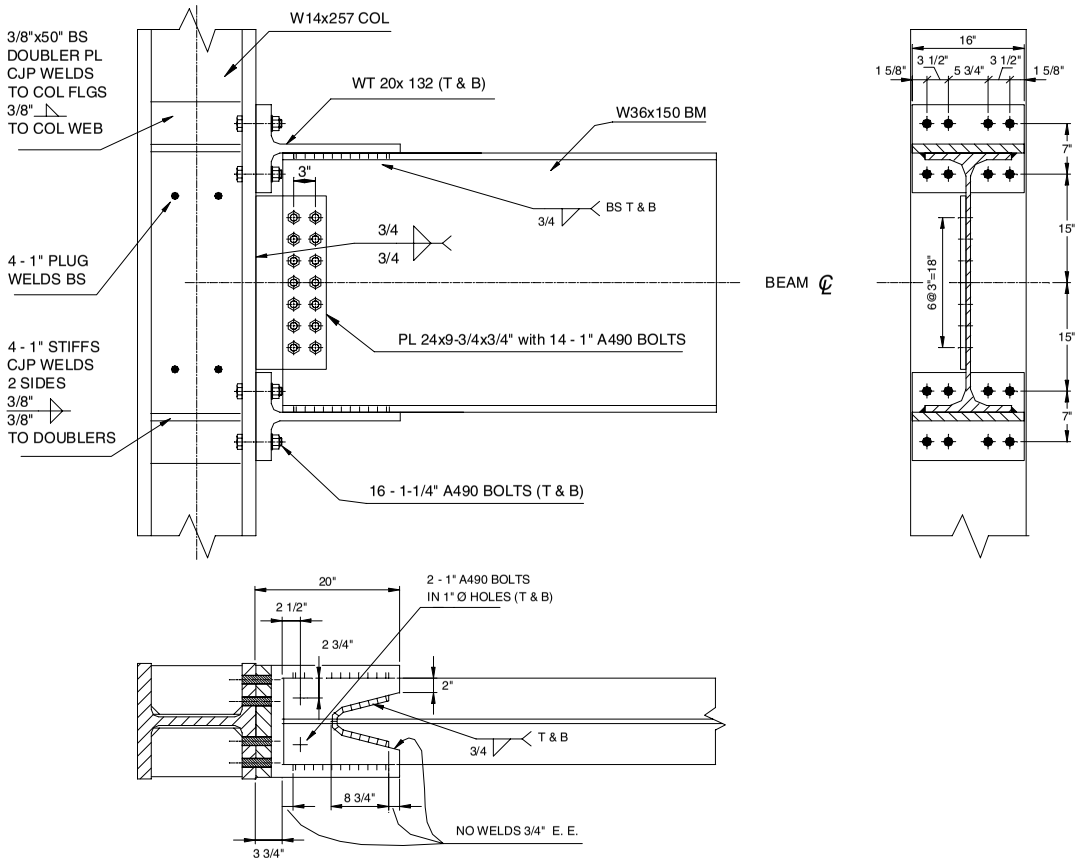

Figure 1-7. Design details of Specimen 2

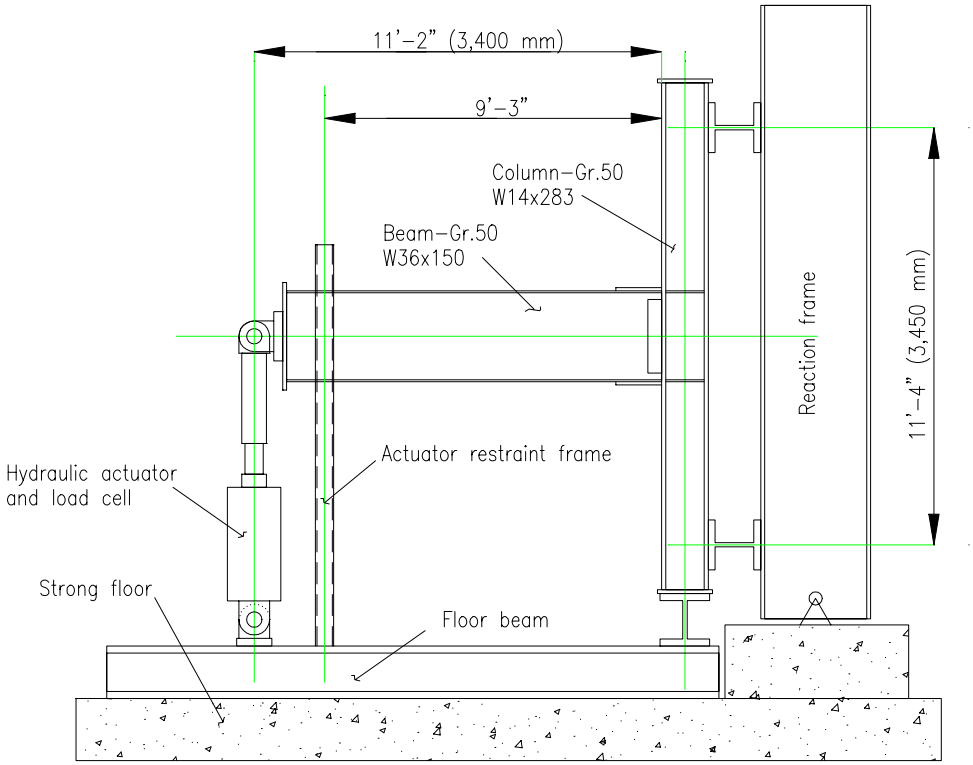

Figure 2-1. Test setup for both specimens

Figure 2-2. View of a test in progress

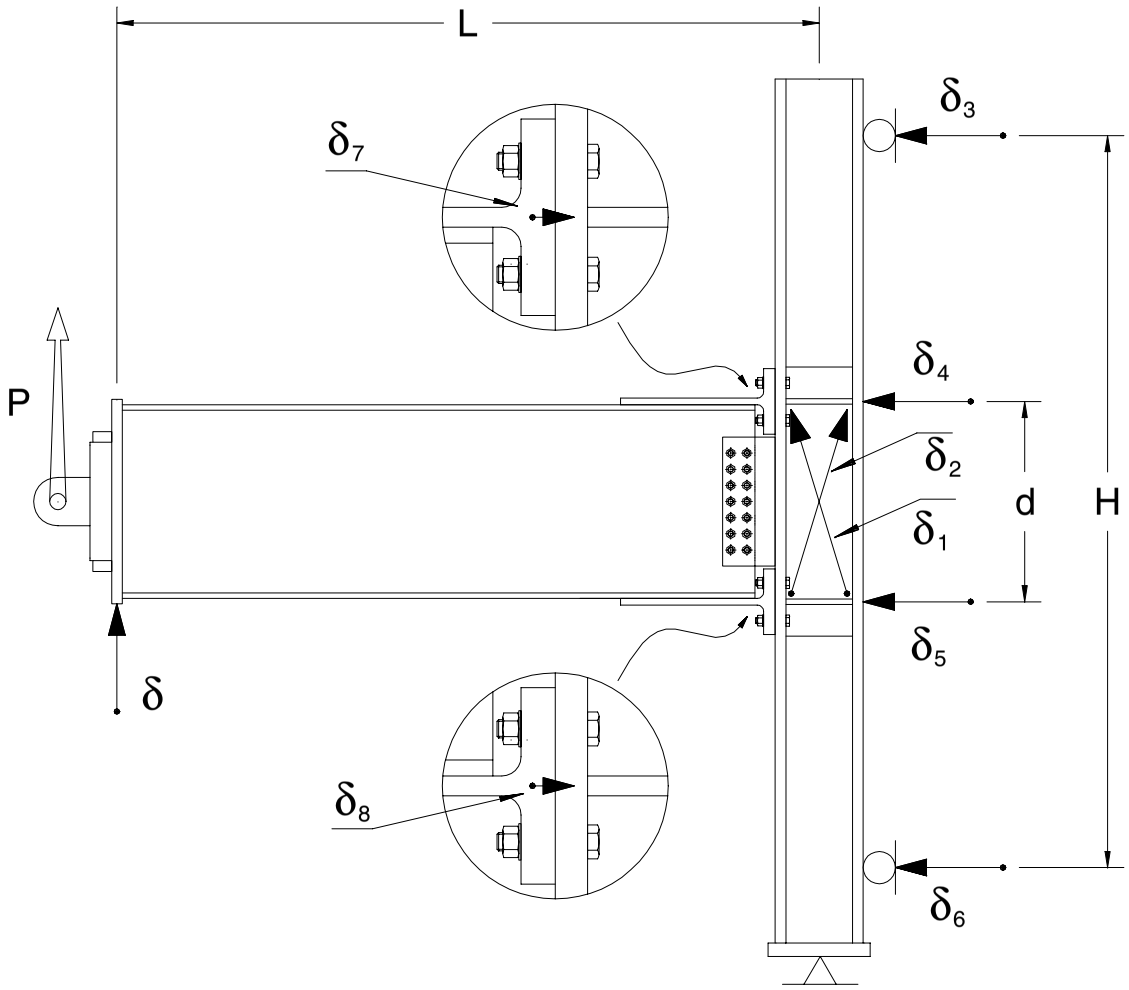

Figure 2-3. Reference dimensions and measurements for the test specimens

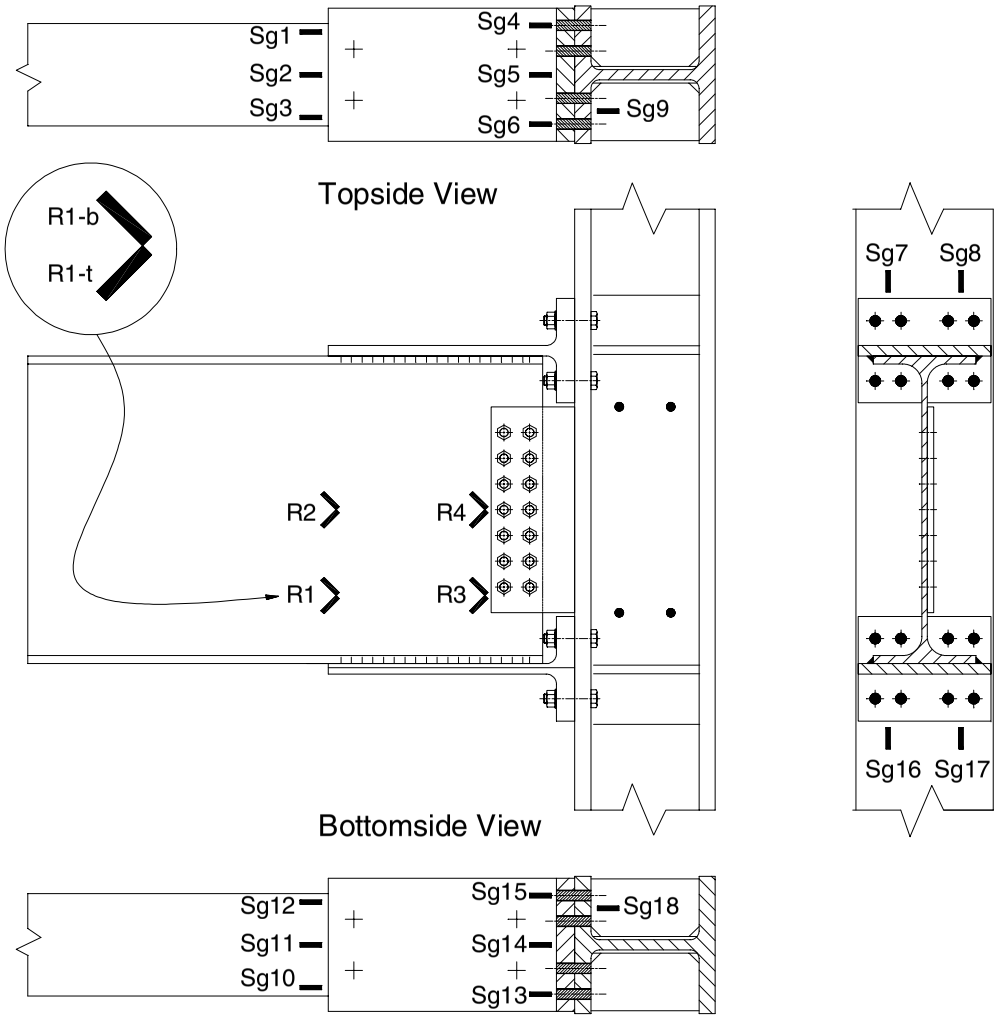

Figure 2-4. Strain gages and rosettes location for Specimen 1

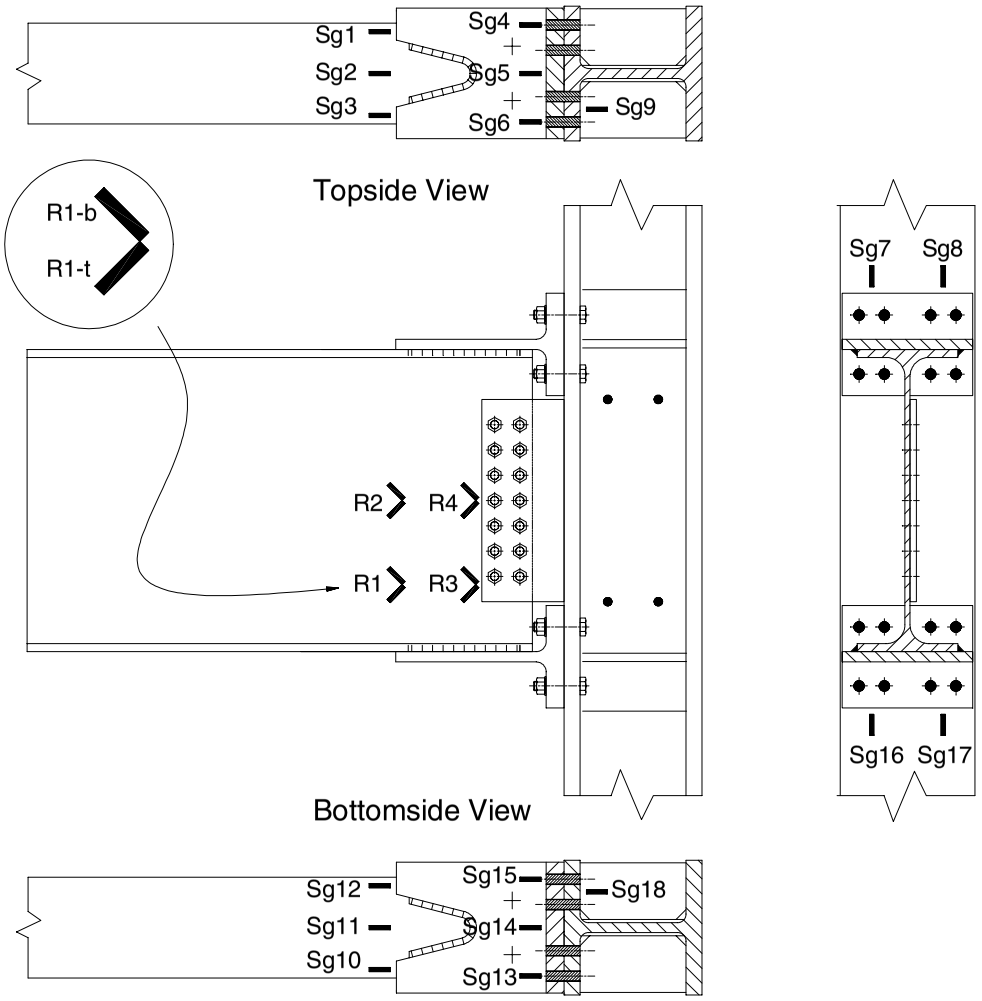

Figure 2-5. Strain gages and rosettes location for Specimen 2

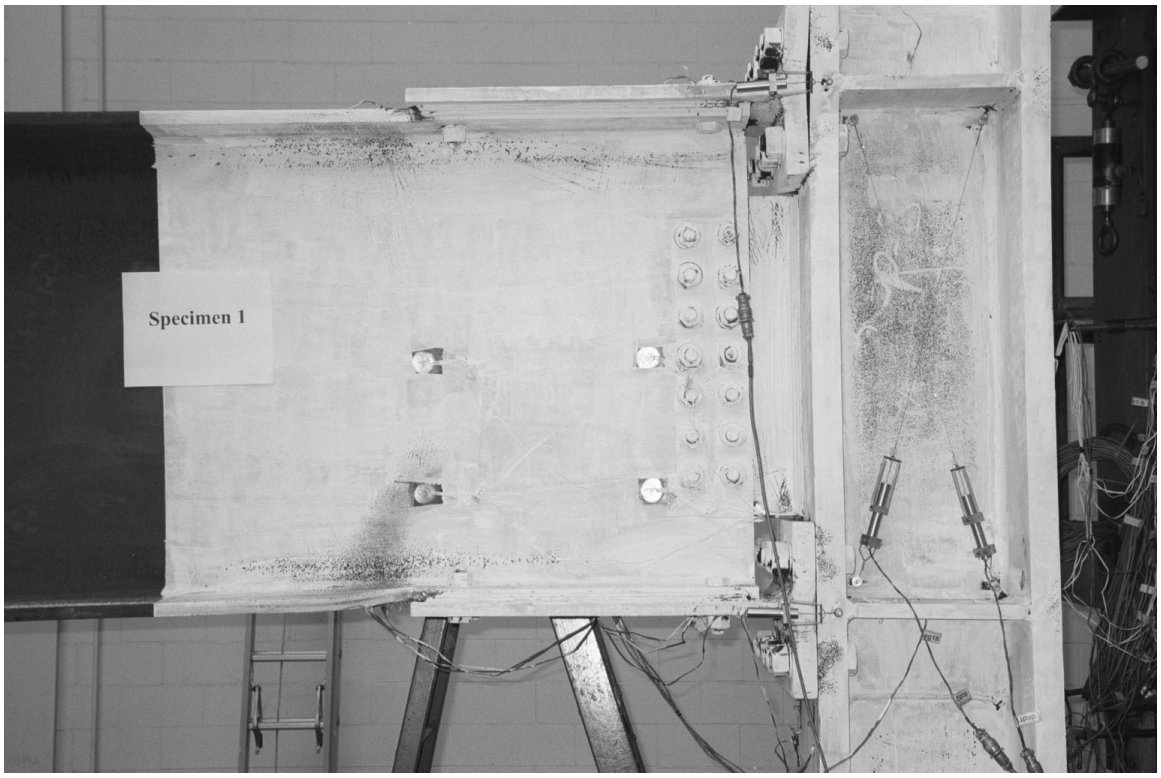

Figure 2-6. Specimen 1 after the test (side view

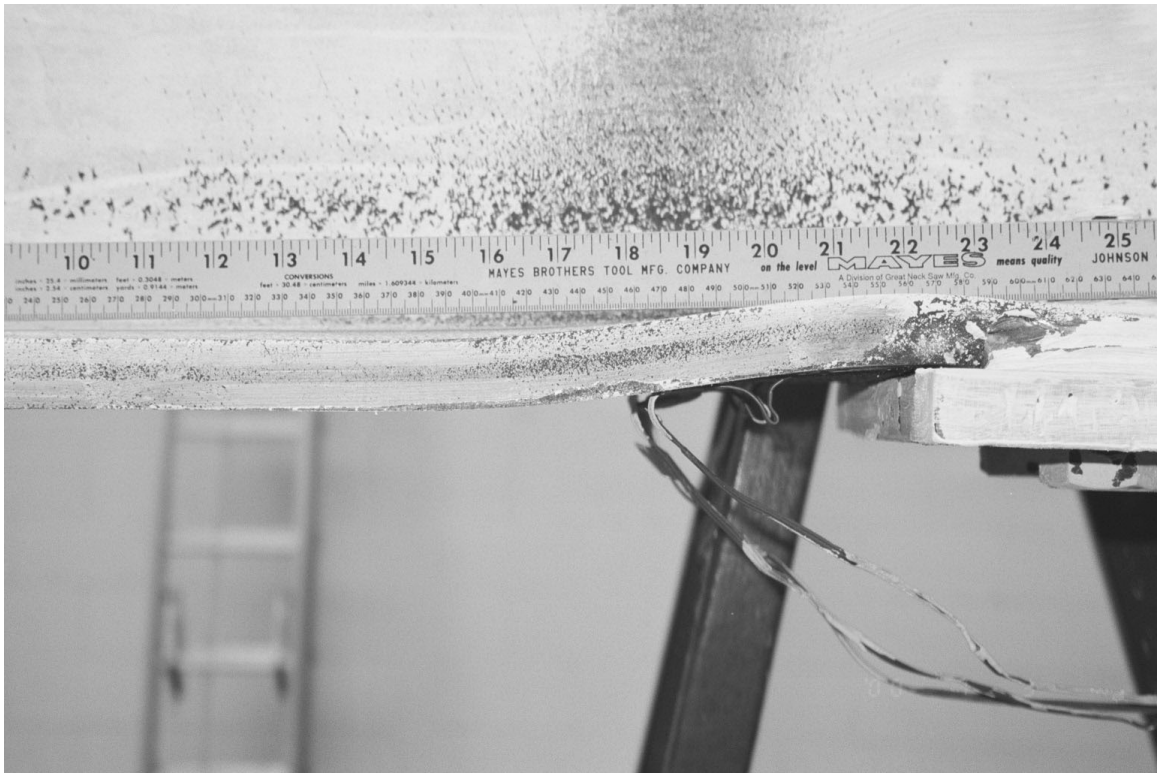

Figure 2-7. Residual beam flange buckling (after the test)

Figure 2-8. Residual beam web buckling (after the test)

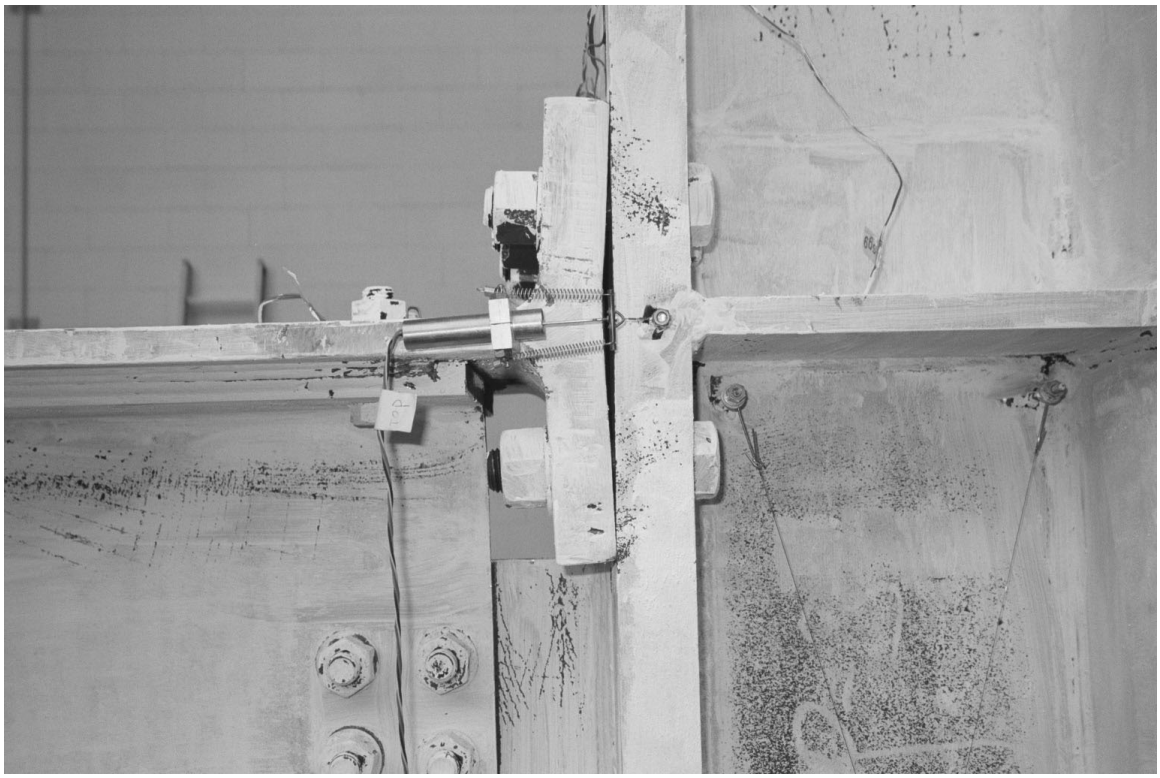

Figure 2-9. Residual gap opening in the upper T-section (after the test)

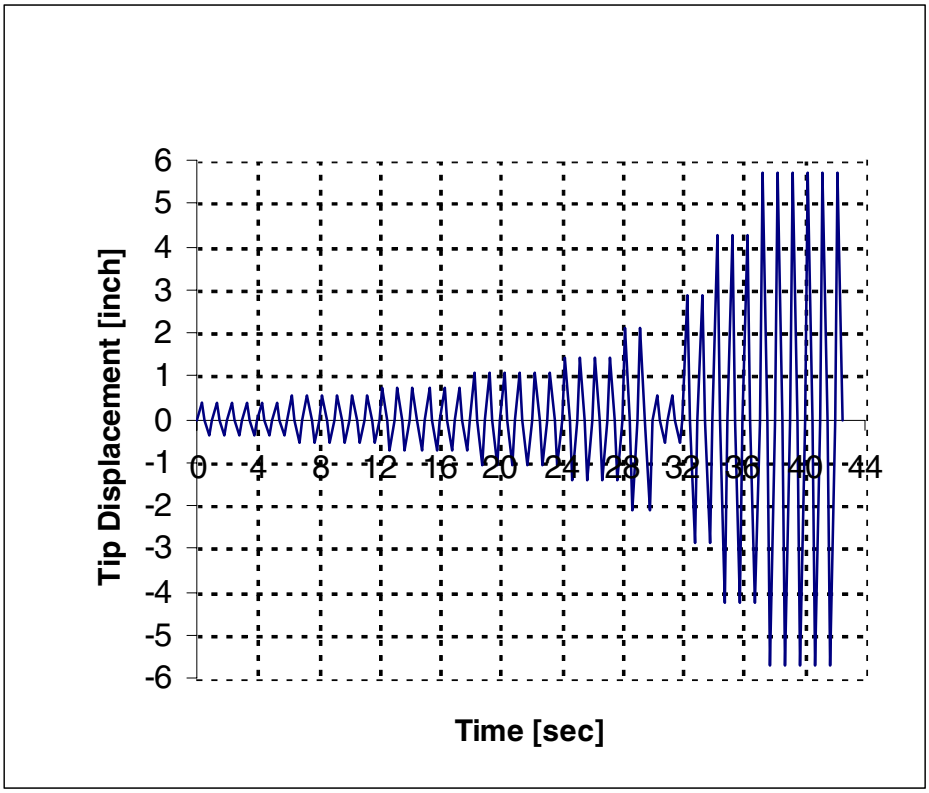

Figure 2-10. Loading history for Specimen 1

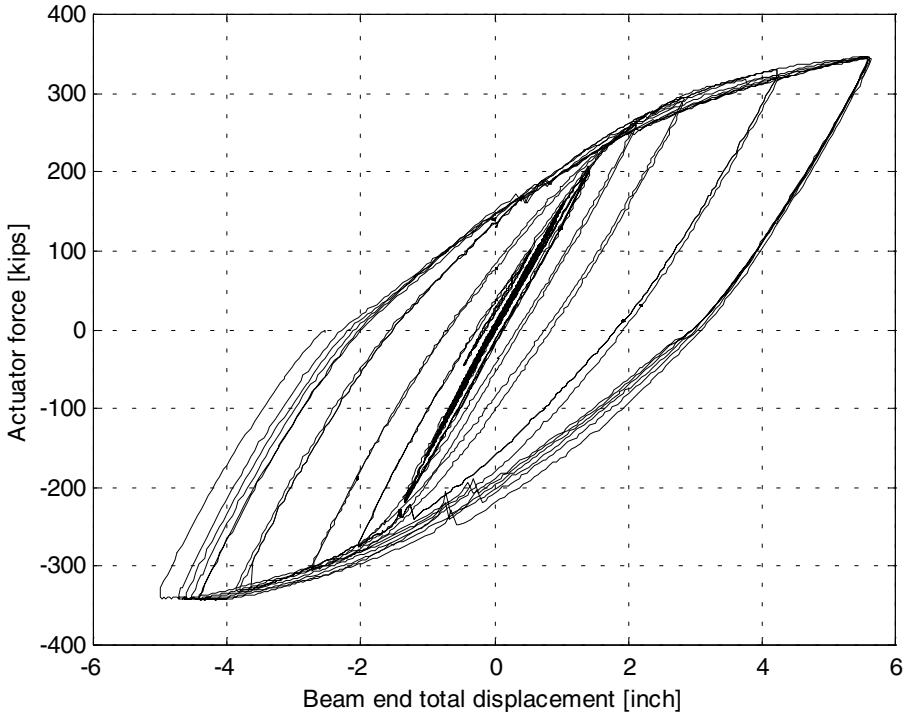

Figure 2-11. Imposed load versus total beam end displacement for Specimen 1

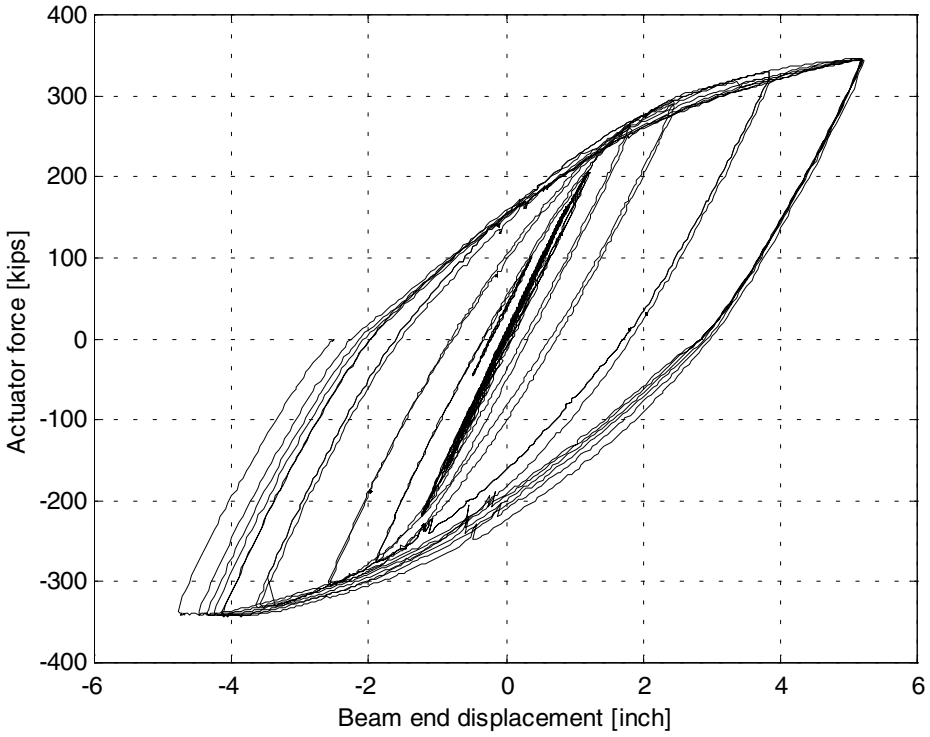

Figure 2-12. Imposed load versus beam end displacement for Specimen 1

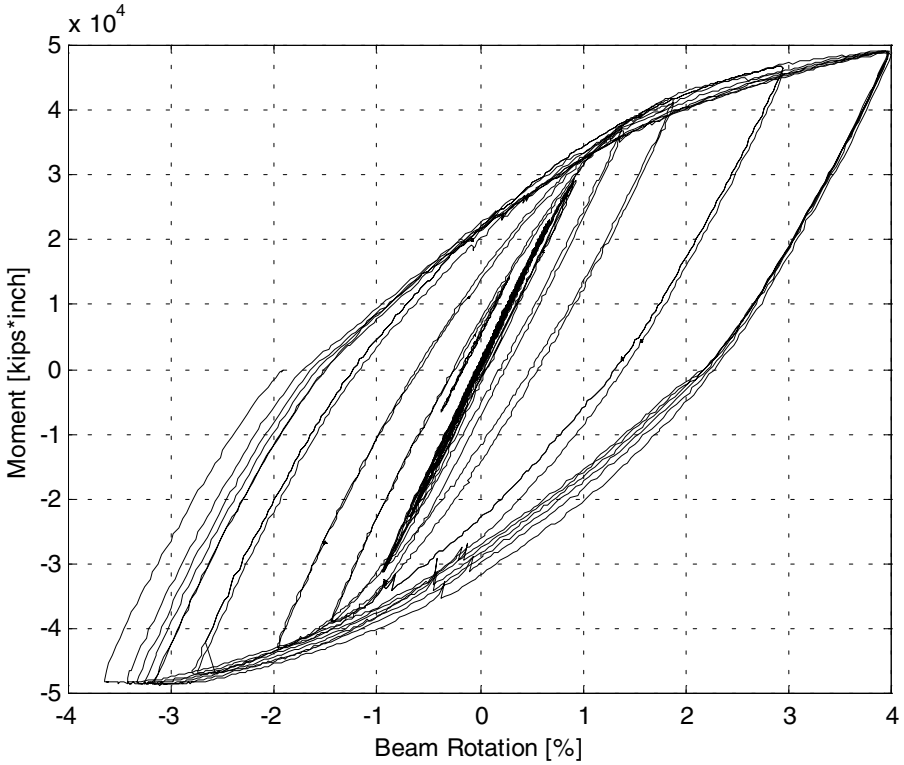

Figure 2-13. Moment versus beam total rotation for Specimen 1

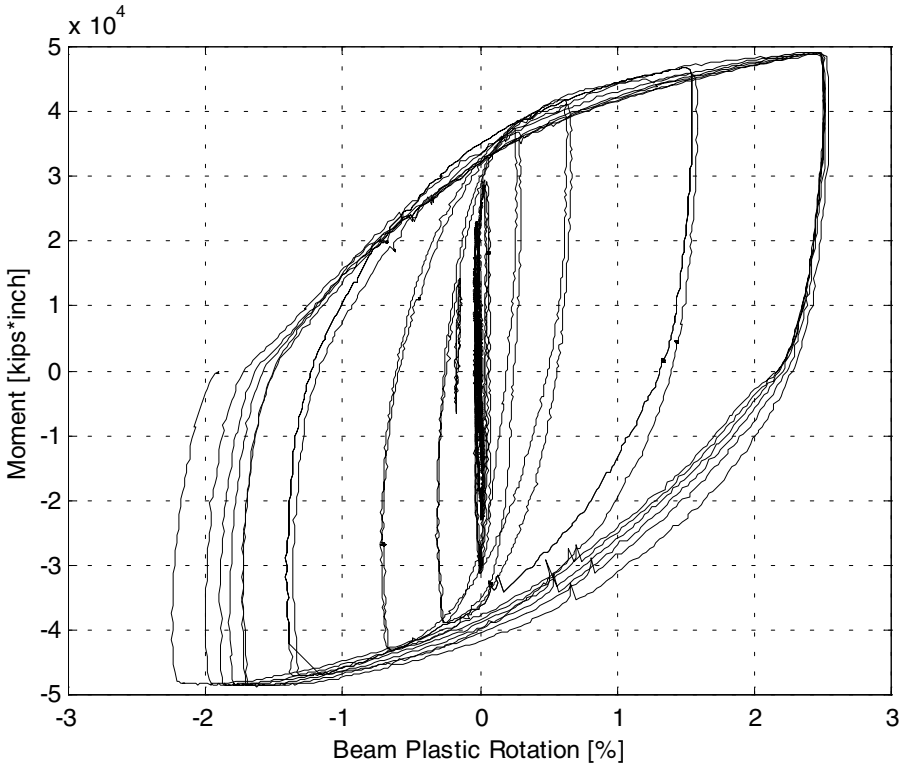

Figure 2-14. Moment versus beam plastic rotation for Specimen 1

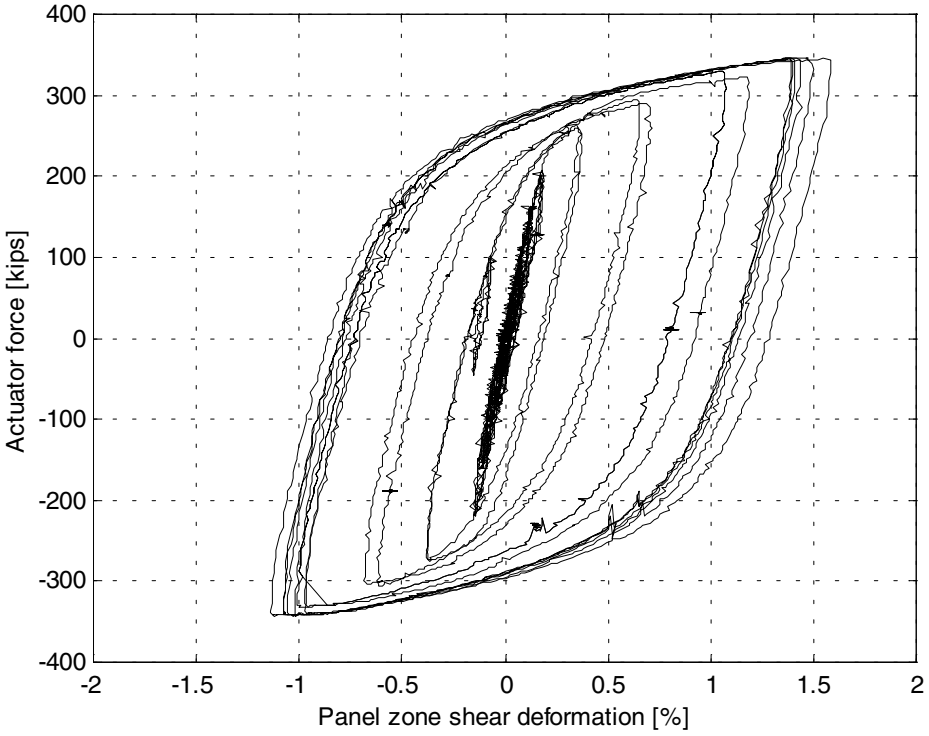

Figure 2-15. Imposed load versus deformation in panel zone for Specimen 1

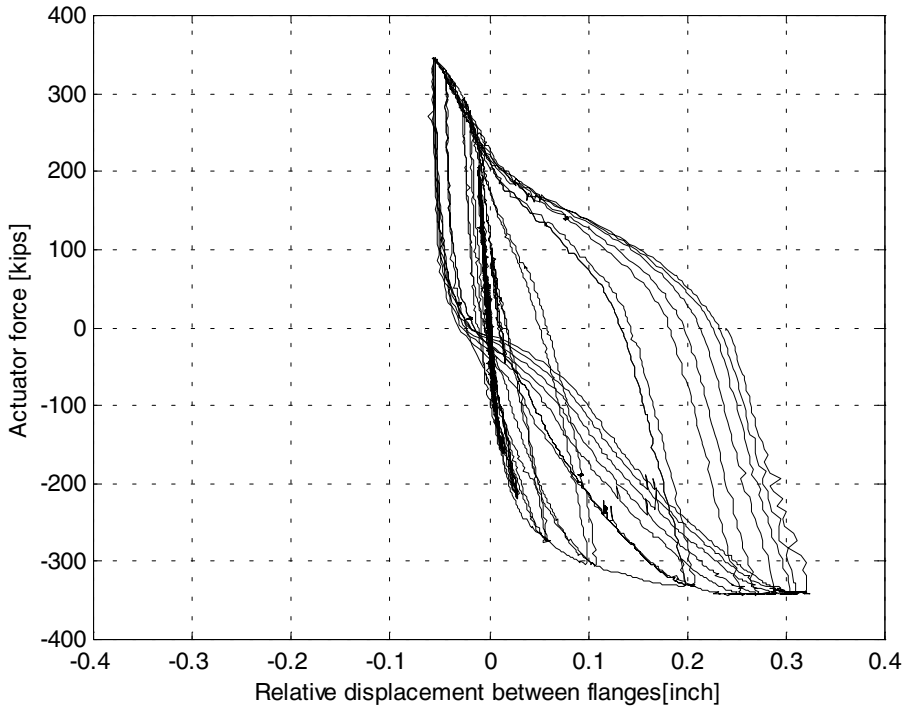

Figure 2-16a. Relative displacement between column and top T-section flanges for Specimen 1

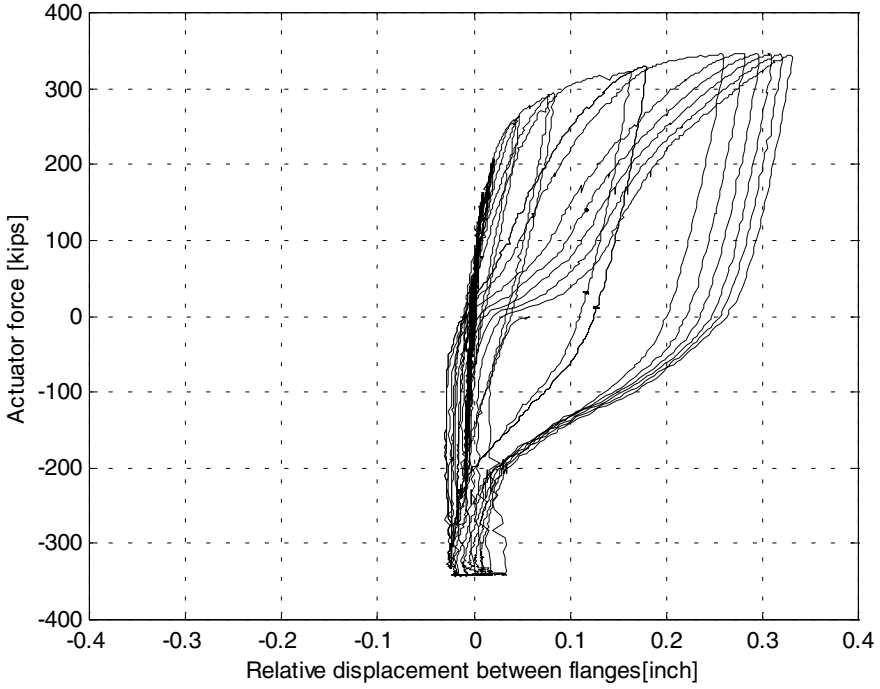

Figure 2-16b. Relative displacement between column and bottom T-section flanges for Specimen 1

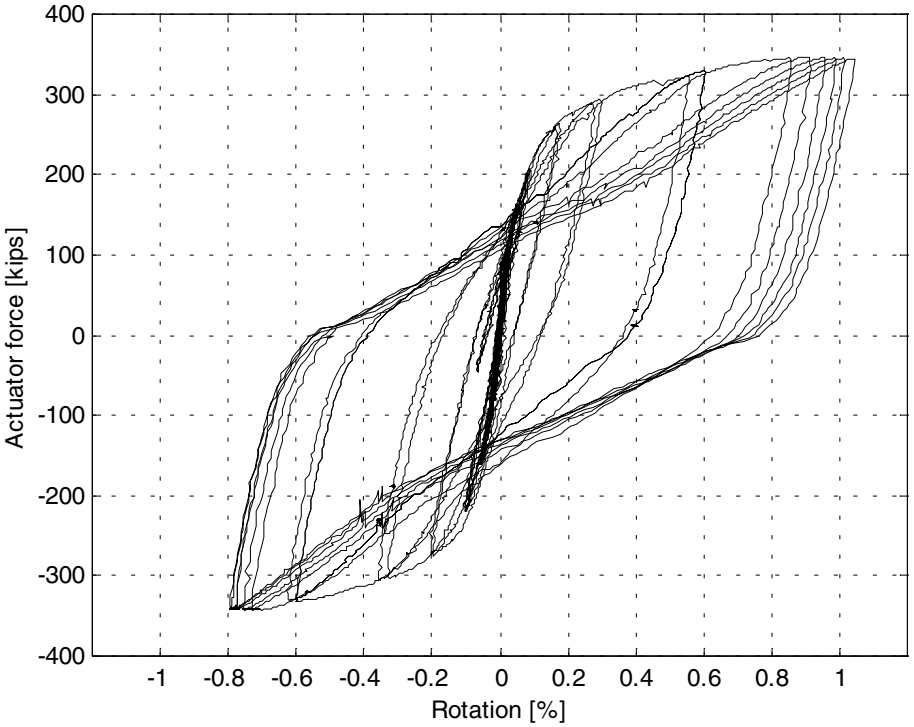

Figure 2-17. Imposed load versus beam rotation due gap opening in T-section (Specimen 1)

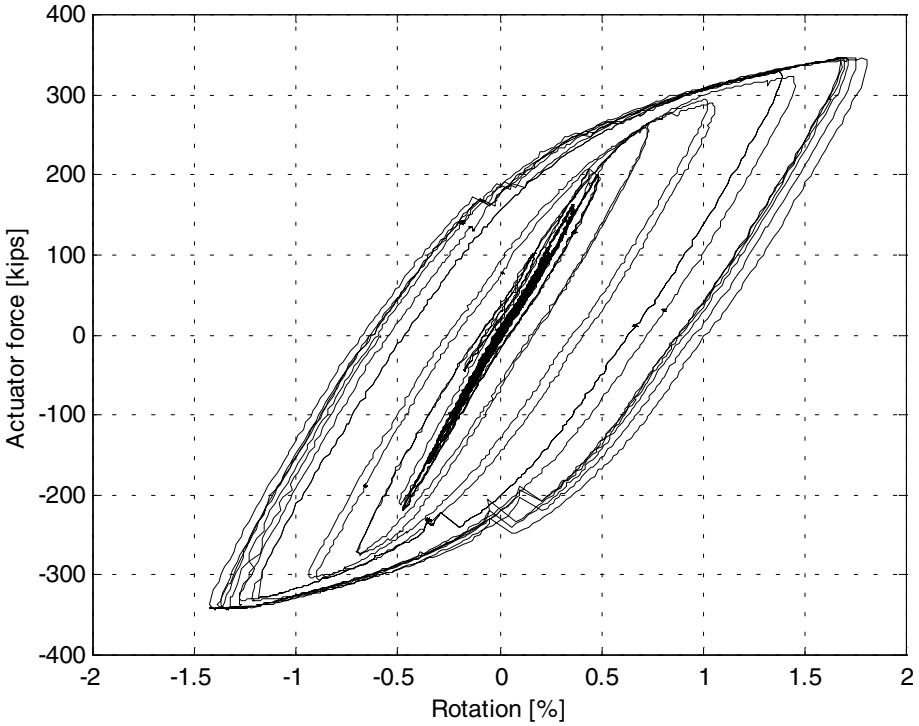

Figure 2-18. Imposed load versus panel zone rotation for Specimen 1

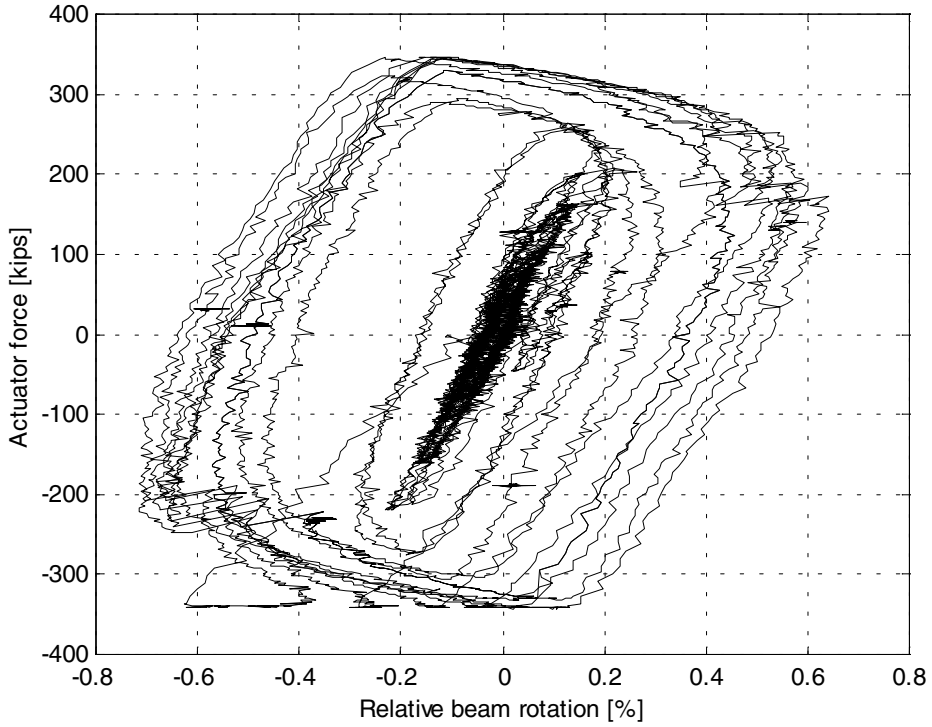

Figure 2-19. Imposed load versus relative beam rotation for Specimen 1

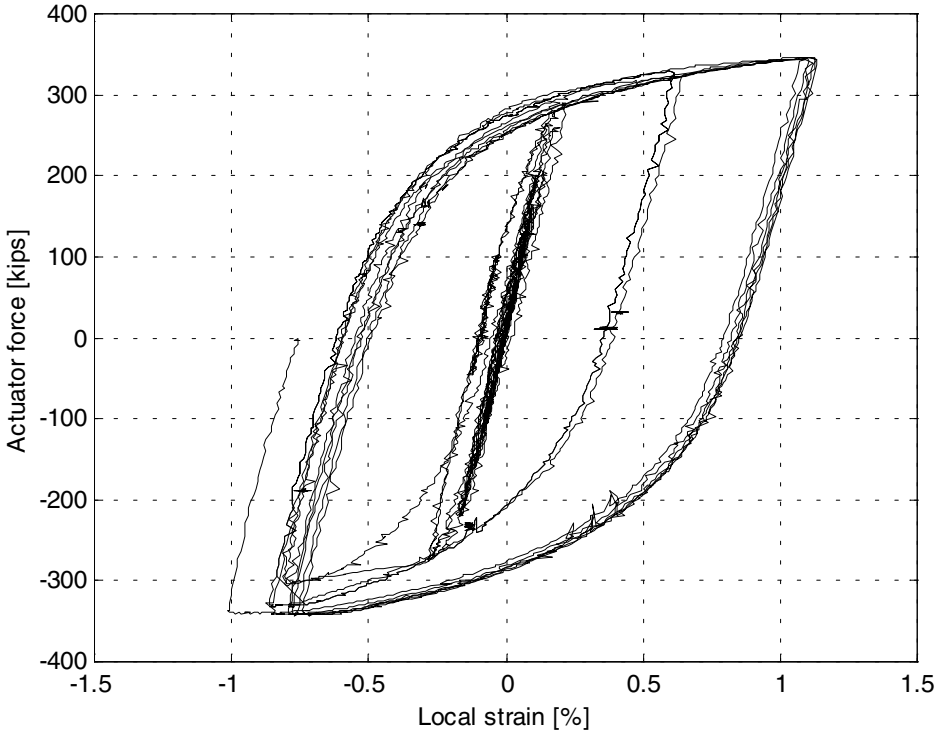

Figure 2-20. Local strain at SG2 location for Specimen 1

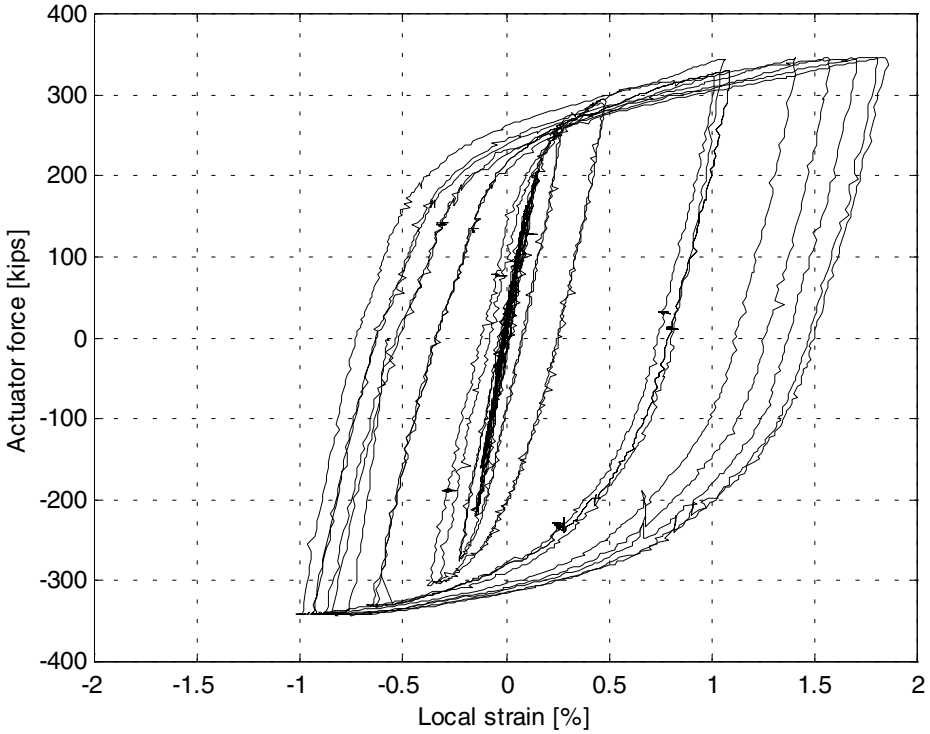

Figure 2-21. Local strain at SG4 location for Specimen 1

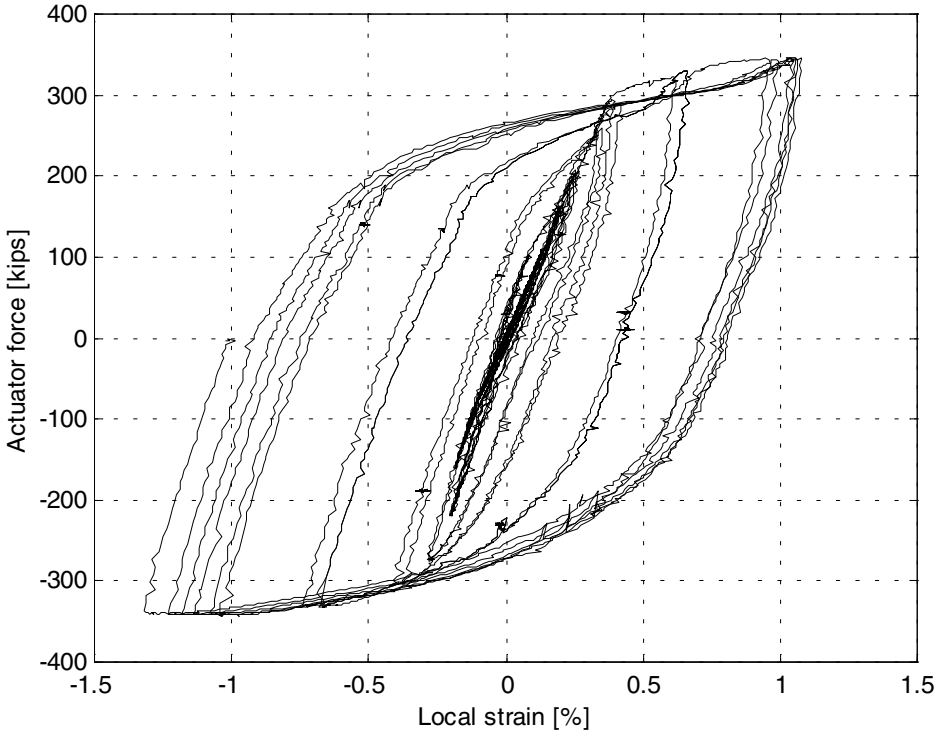

Figure 2-22. Local strain at SG5 location for Specimen 1

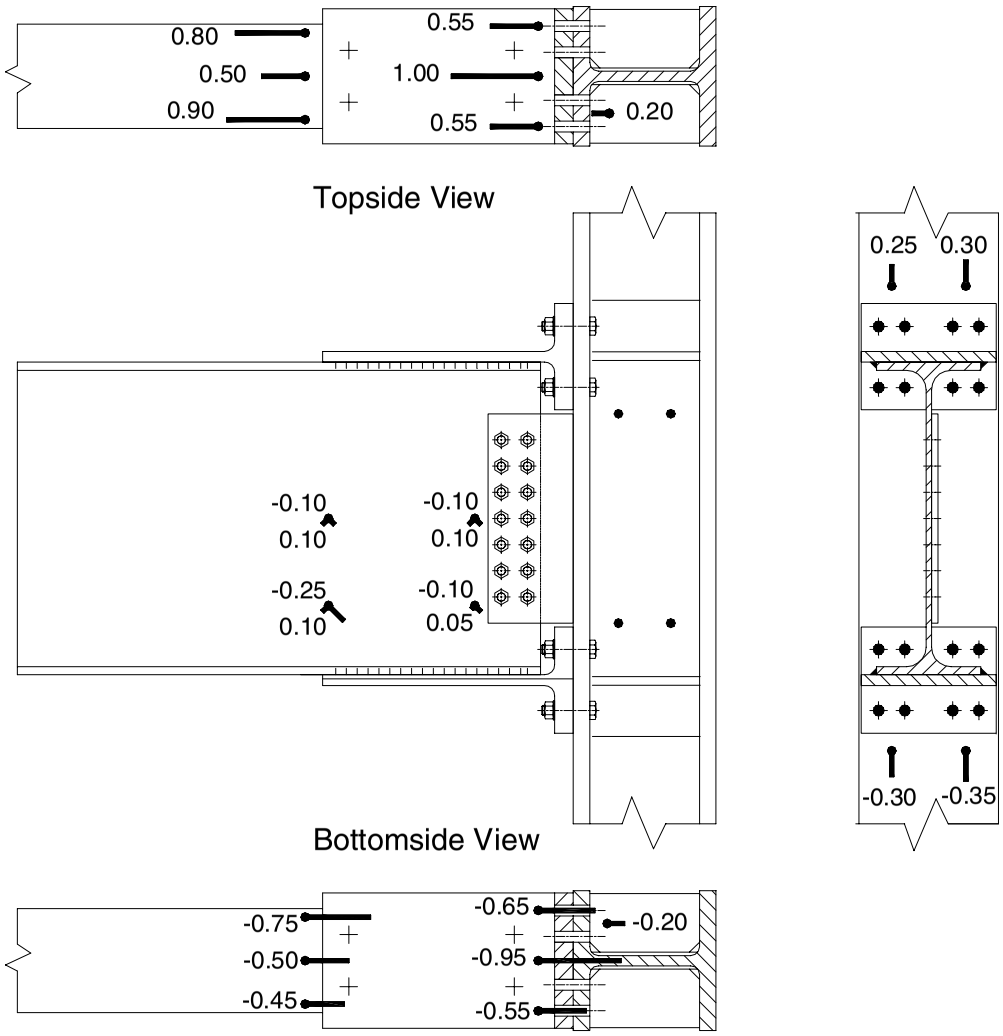

Figure 2-23. Specimen 1: normalized strain data at 1.02″ beam end displacement (max. value 0.20 %)

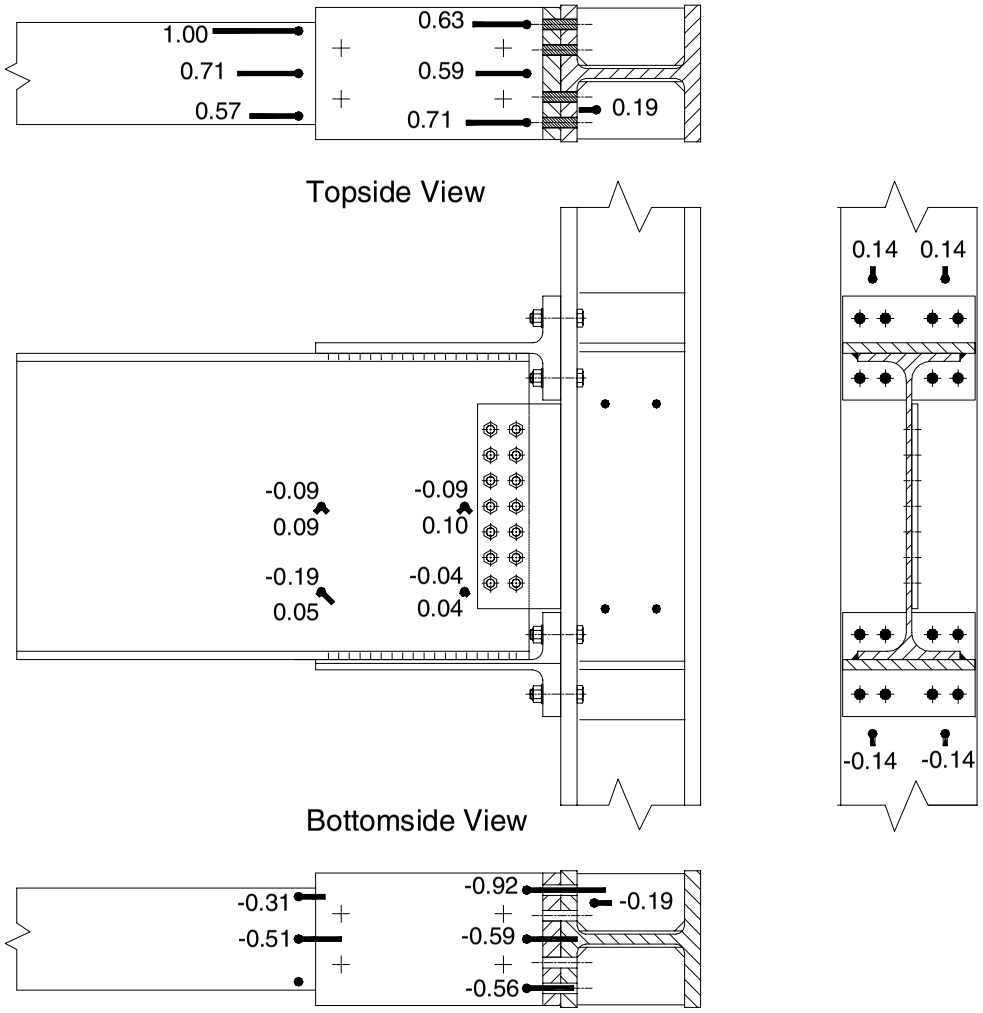

Figure 2-24. Specimen 1: normalized strain data at 2.85″ beam end displacement (max. value 0.70 %)

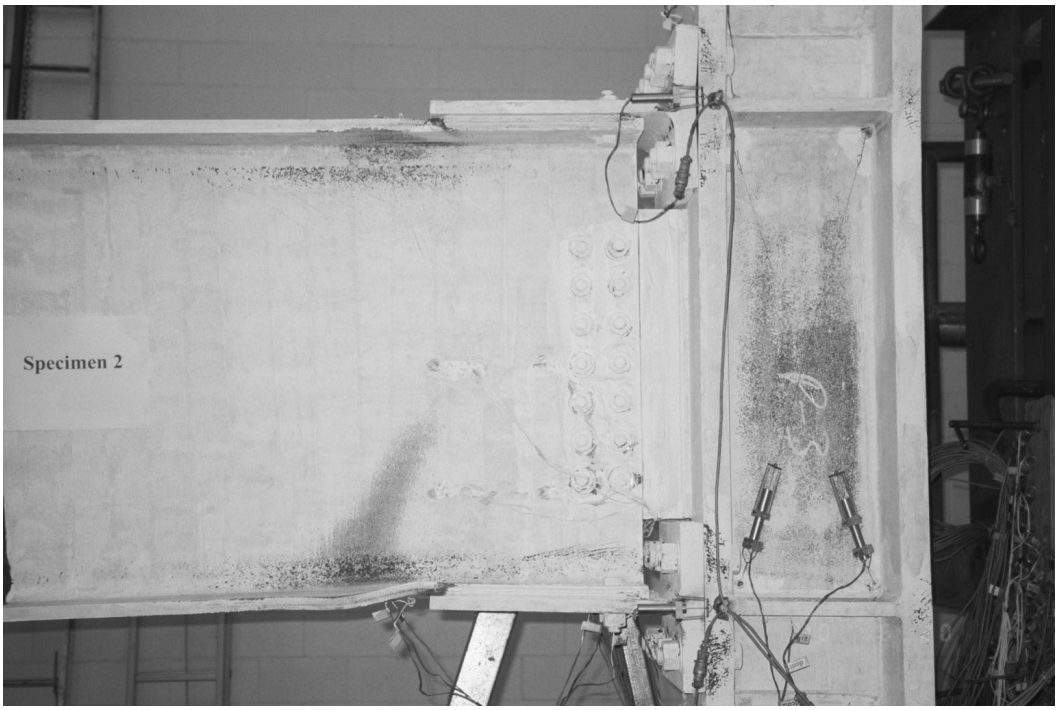

Figure 2-25. Specimen 2 after the test (side view)

Figure 2-26. Specimen 2: residual gap opening in top T-section

Figure 2-27. Specimen 2: top beam flange buckling

Figure 2-28. Specimen 2: bottom beam flange buckling

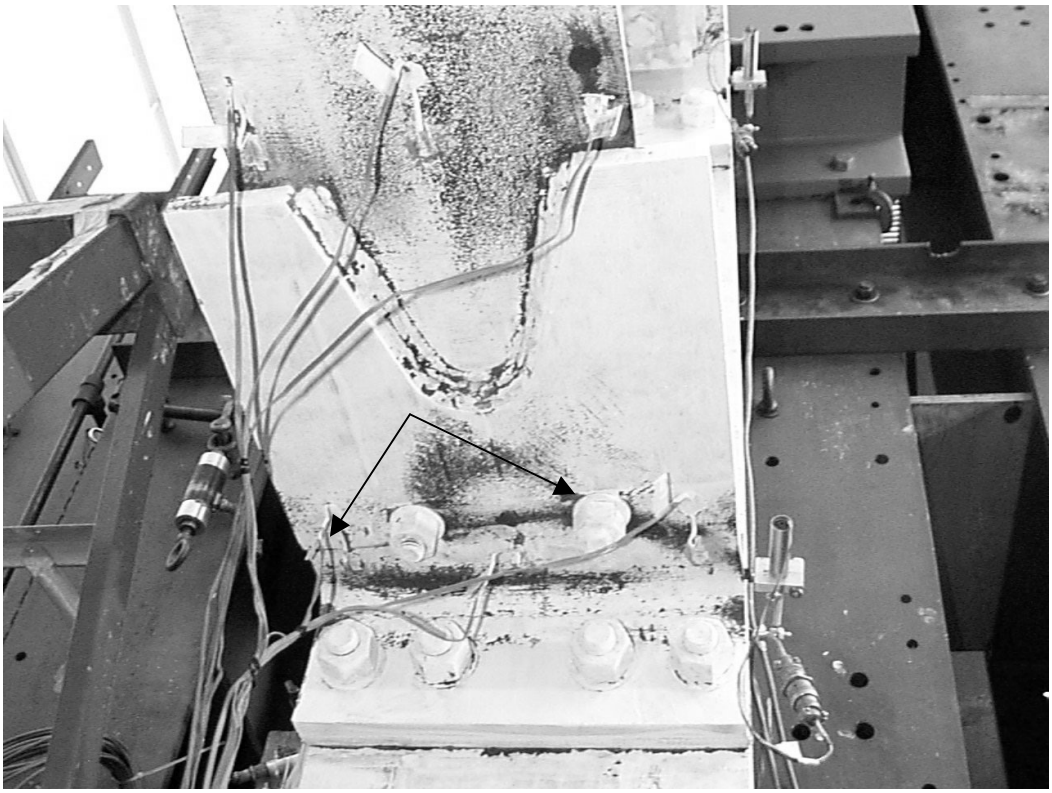

Figure 2-29. Specimen 2: crack line location

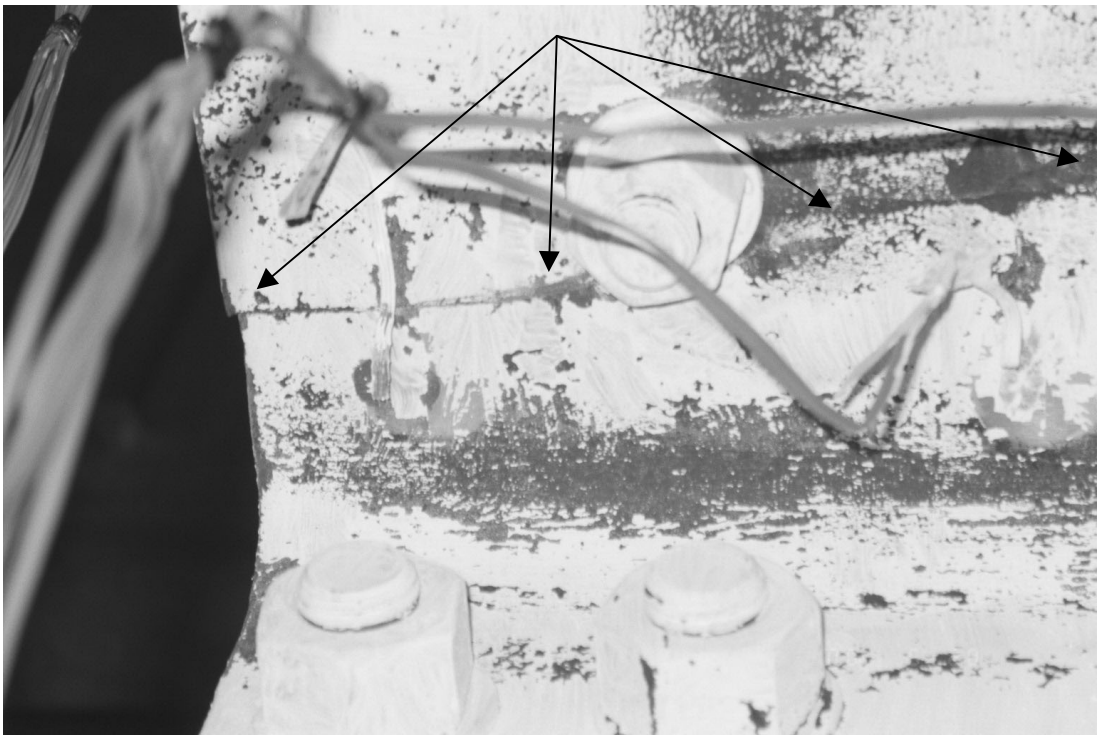

Figure 2-30. Specimen 2: close view of the crack line

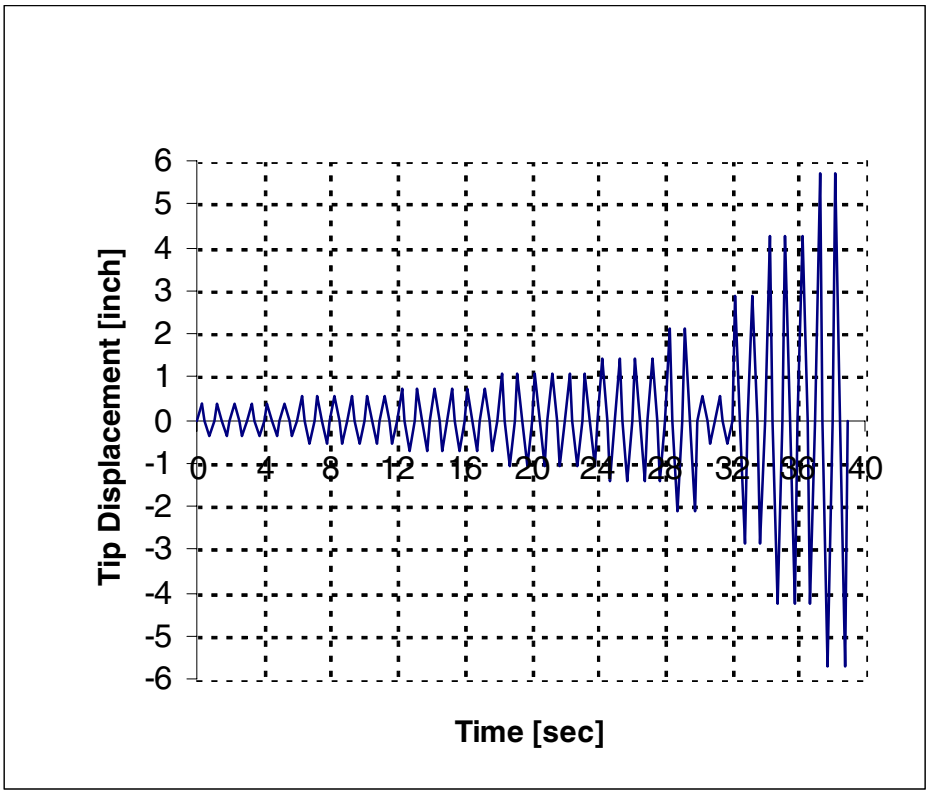

Figure 2-31. Loading history for Specimen 2

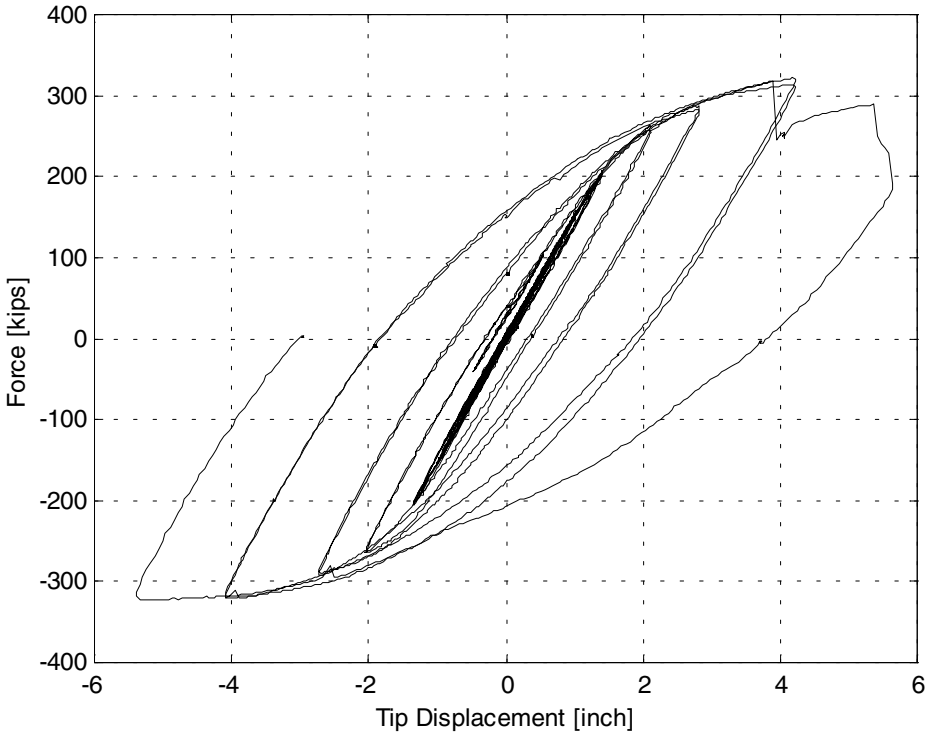

Figure 2-32. Imposed load versus total beam end displacement (Specimen 2)

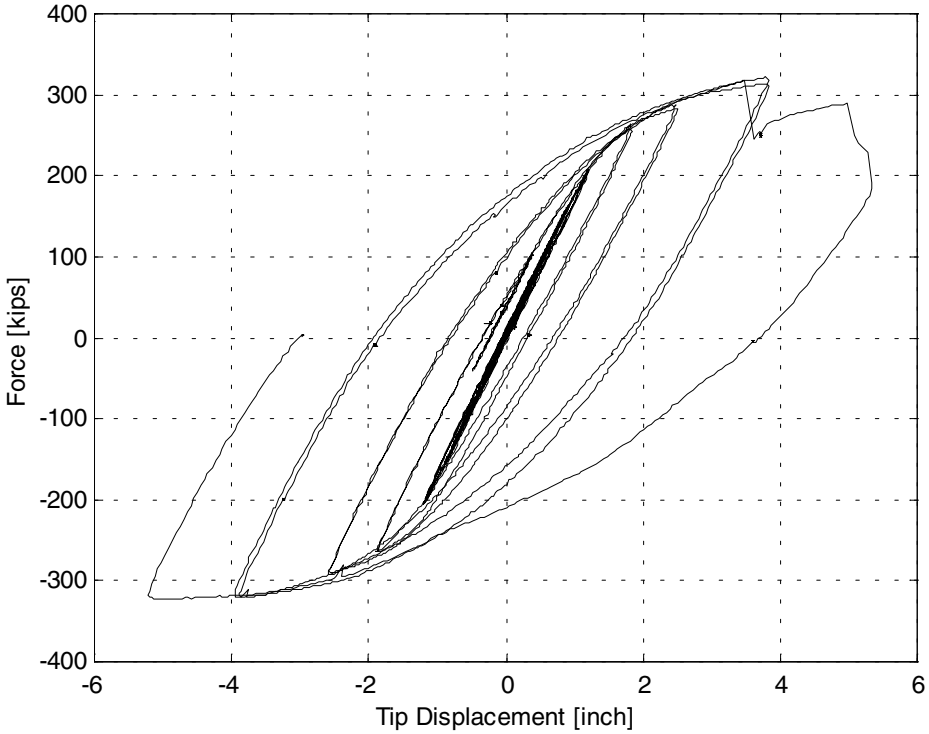

Figure 2-33. Imposed load versus beam end displacement (Specimen 2)

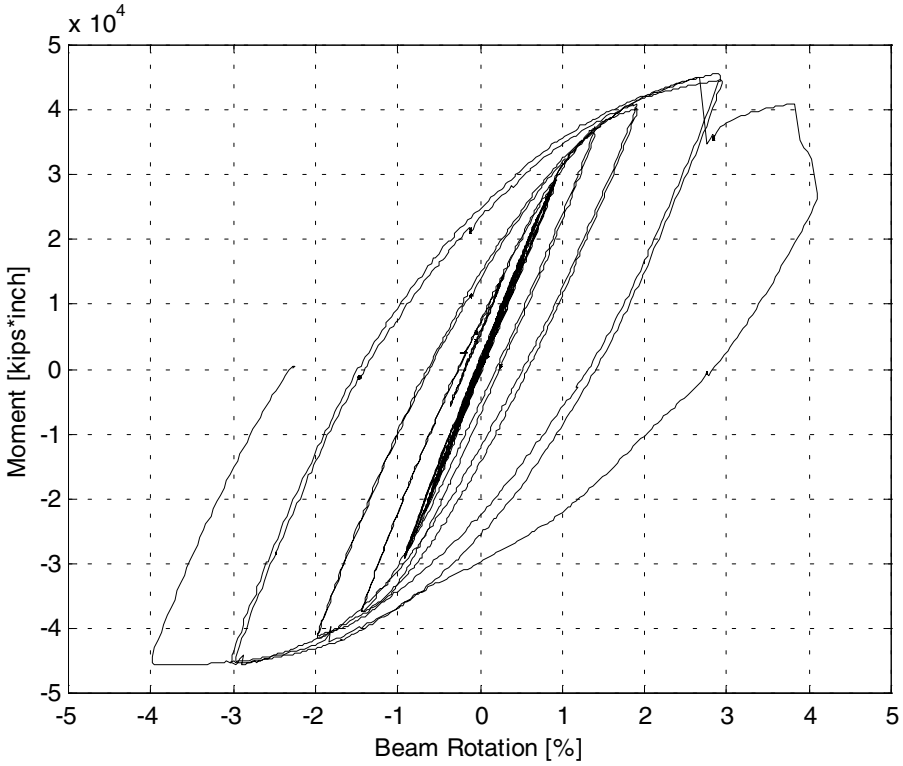

Figure 2-34. Moment versus beam total rotation (Specimen 2)

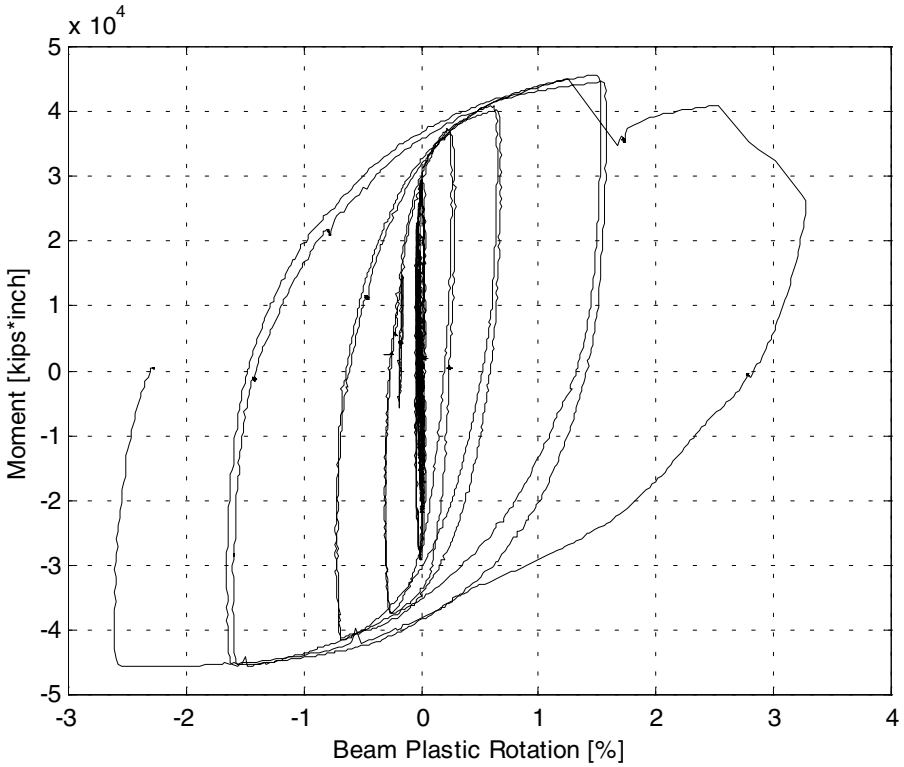

Figure 2-35. Moment versus beam plastic rotation (Specimen 2)

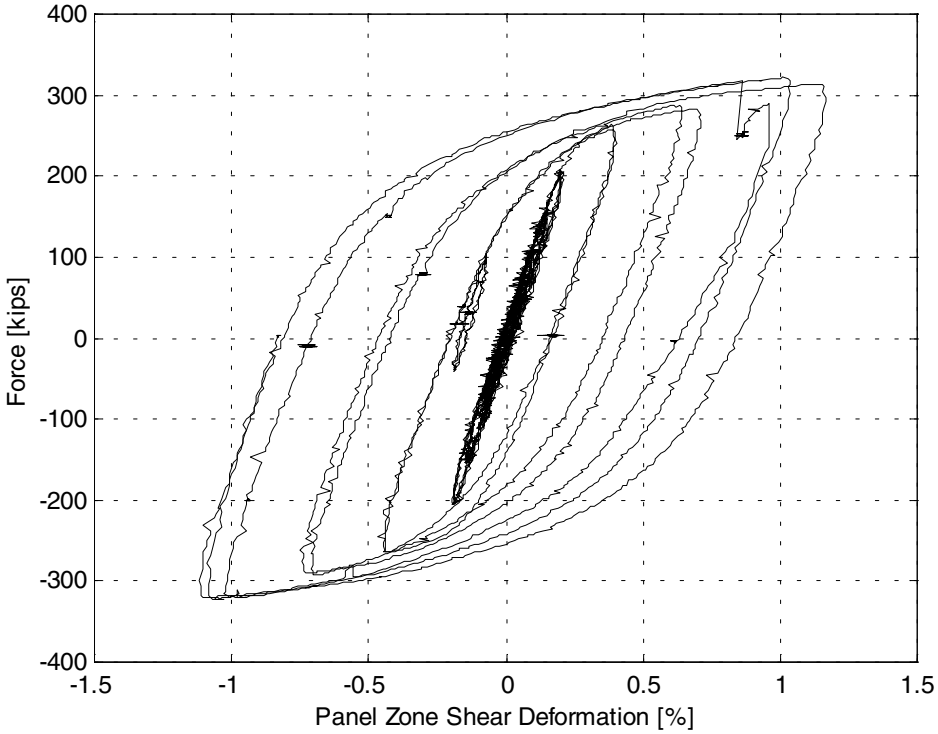

Figure 2-36. Imposed load versus column panel zone deformation (Specimen 2)

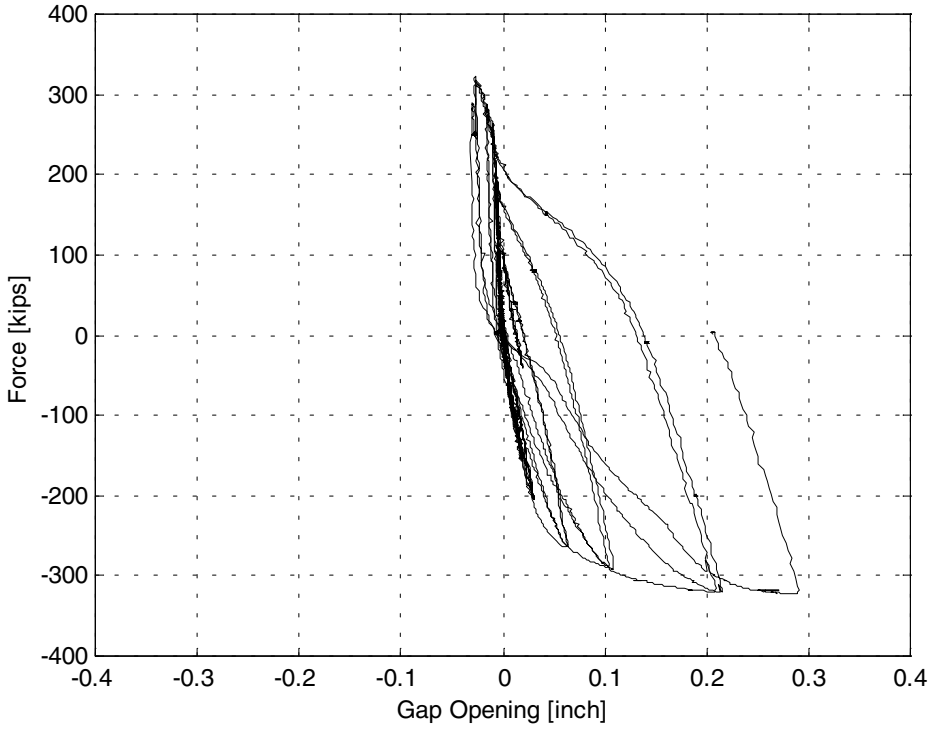

Figure 2-37a. Relative displacement between column and top T-section flanges (Specimen 2)

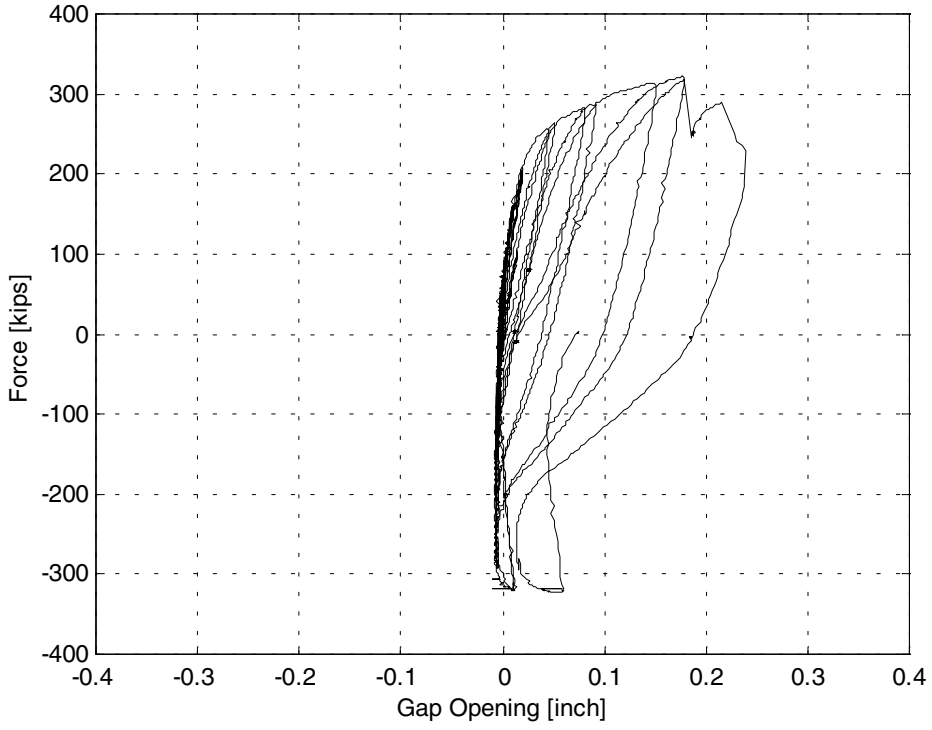

Figure 2-37b. Relative displacement between column and bottom T-section flanges (Specimen 2)

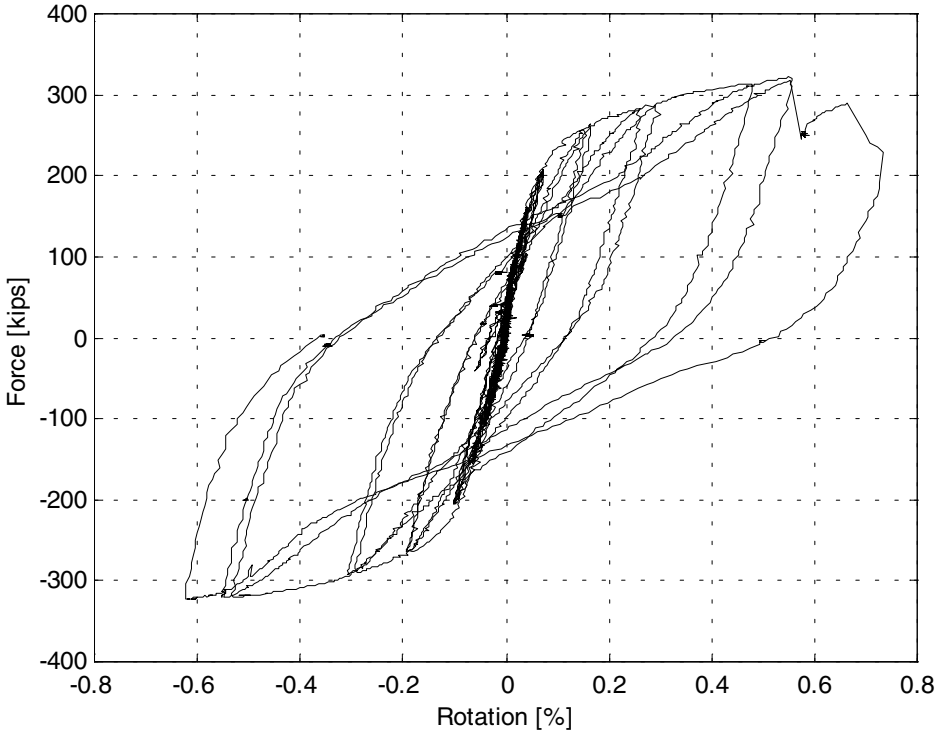

Figure 2-38. Imposed load versus beam rotation due gap opening in T-sections (Specimen 2)

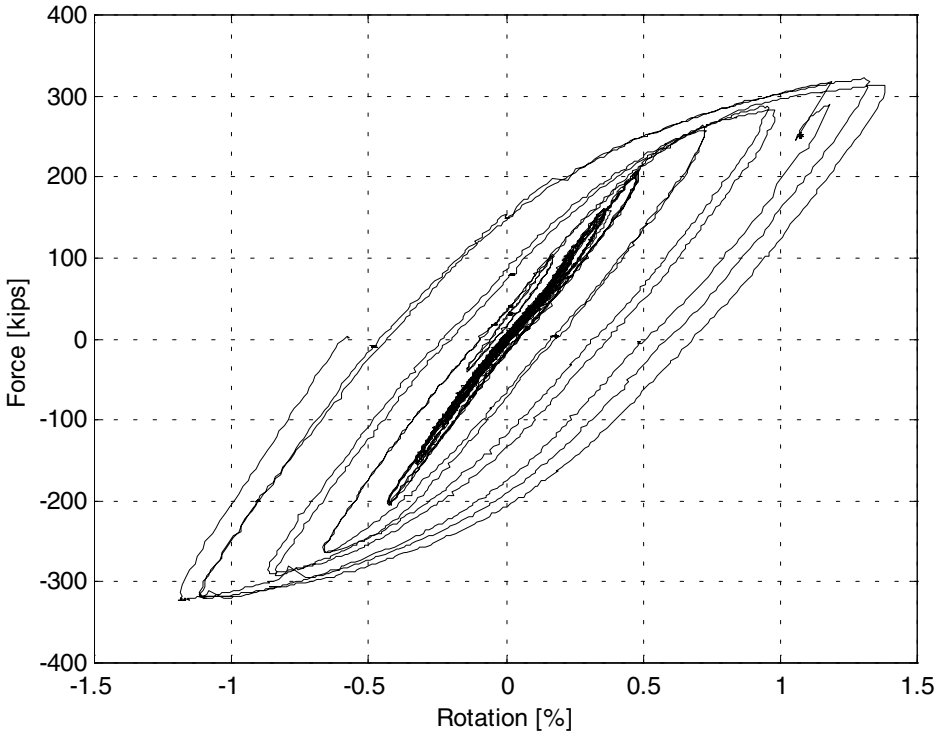

Figure 2-39. Imposed load versus panel zone rotation for Specimen 2

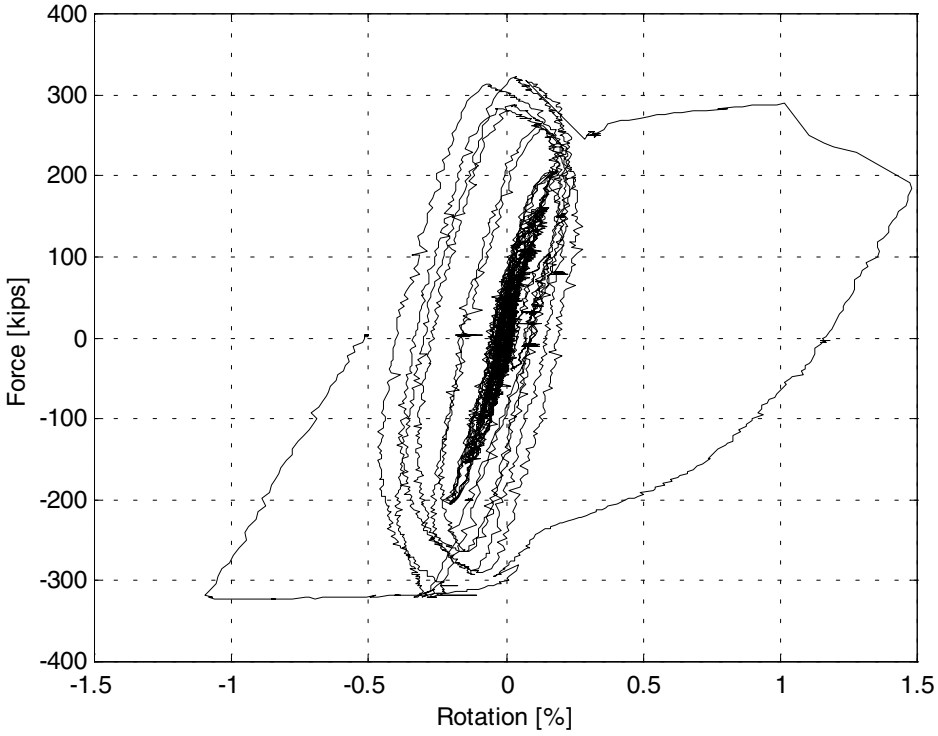

Figure 2-40. Imposed load versus relative beam rotation for Specimen 2

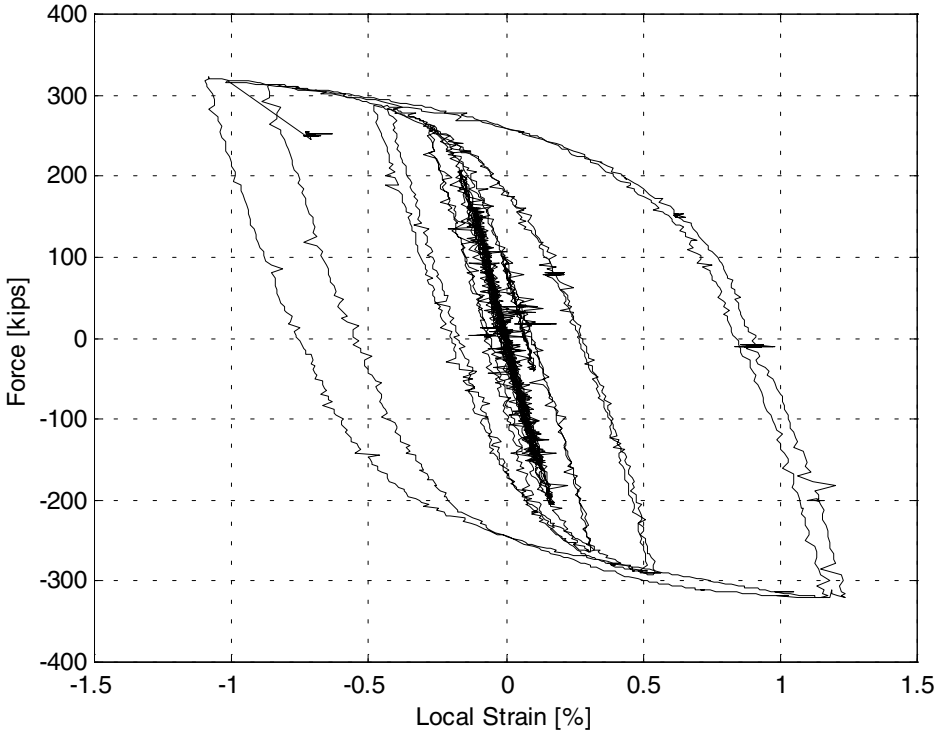

Figure 2-41. Local strain at SG15 location for Specimen 2

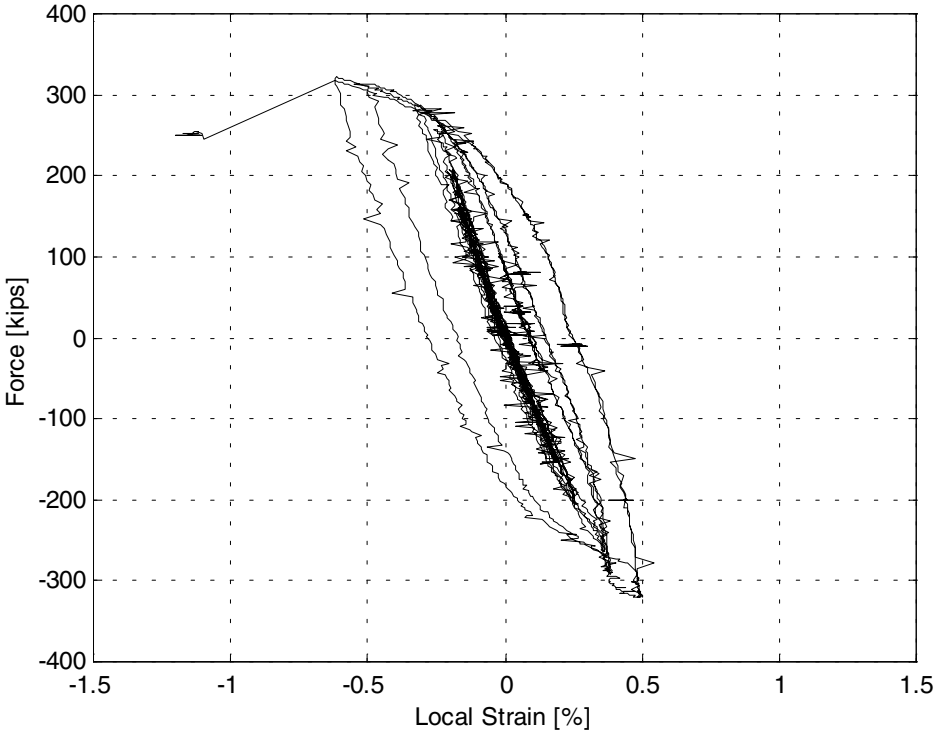

Figure 2-42. Local strain at SG14 location for Specimen 2

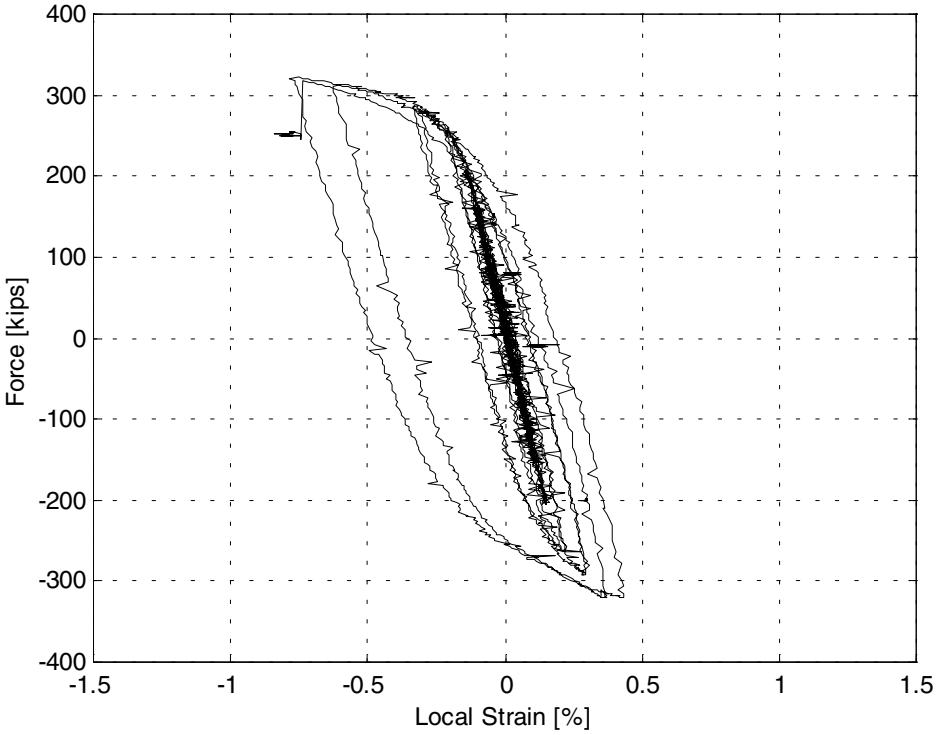

Figure 2-43. Local strain at SG13 location for Specimen 2

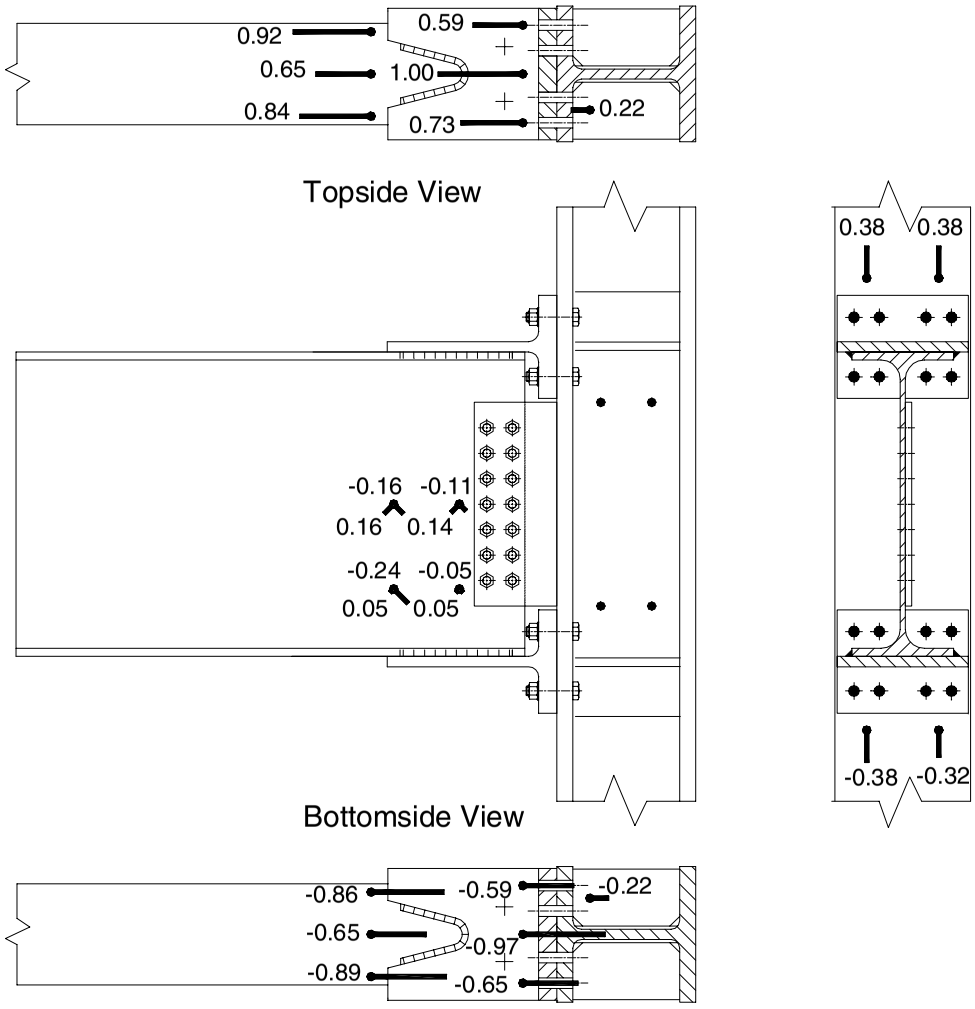

Figure 2-44. Specimen 2: normalized strain data at 1.02″ beam end displacement (max. value 0.18 %)

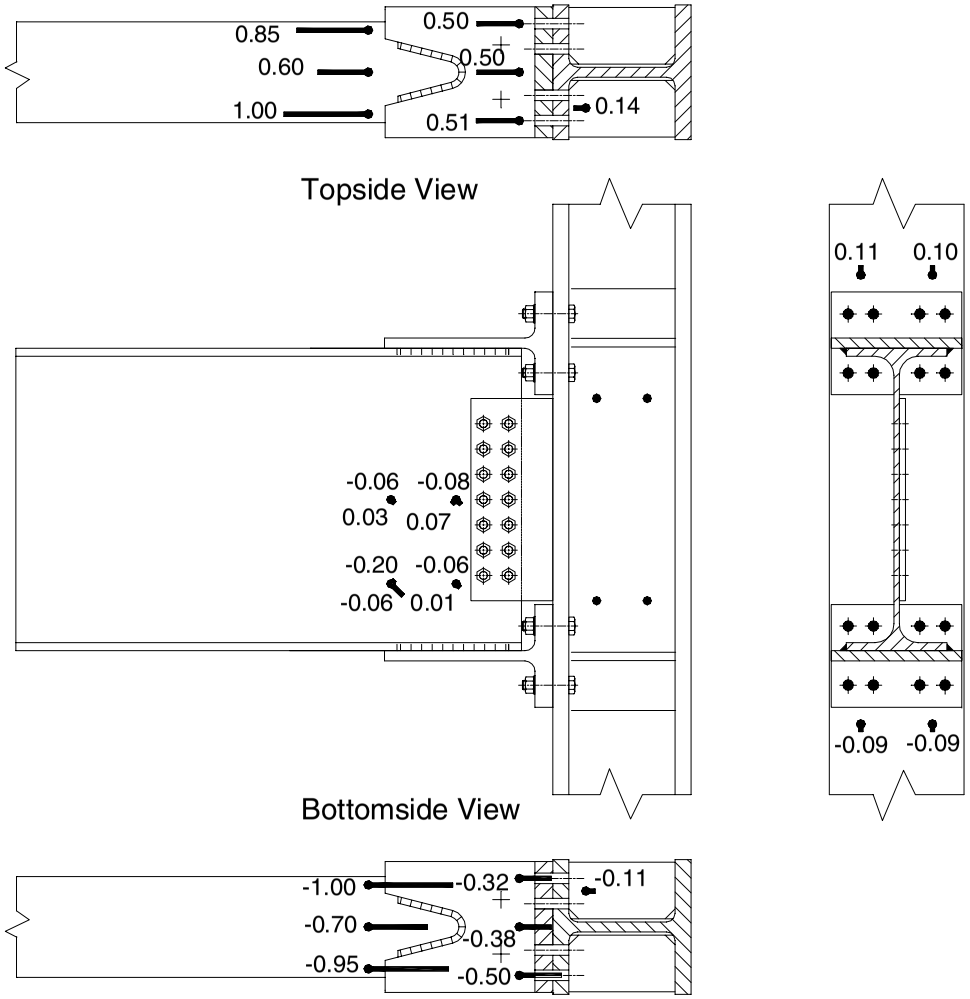

Figure 2-45. Specimen 2: normalized strain data at 2.85″ beam end displacement (max. value 1.00 %)

PEER REPORTS

PEER reports are available from the National Information Service for Earthquake Engineering (NISEE). To order PEER reports, please contact the Pacific Earthquake Engineering Research Center, 1301 South 46th Street, Richmond, California 94804-4698. Tel.: (510) 231-9468; Fax: (510) 231-9461.

PEER 2001/03 *A Modal Pushover Analysis Procedure to Estimate Seismic Demands for Buildings: Theory and Preliminary Evaluation.* Anil K. Chopra and Rakesh K. Goel. January 2001. $15.00

PEER 2001/01 *Experimental Study of Large Seismic Steel Beam-to-Column Connections.* Egor P. Popov and Shakhzod M. Takhirov. November 2000. $15.00

PEER 2000/07 *Cover-Plate and Flange-Plate Reinforced Steel Moment-Resisting Connections.* Taejin Kim, Andrew S. Whittaker, Amir S. Gilani, Vitelmo V. Bertero, and Shakhzod M. Takhirov. September 2000. $33.00

PEER 2000/06 *Seismic Evaluation and Analysis of 230-kV Disconnect Switches.* Amir S. J. Gilani, Andrew S. Whittaker, Gregory L. Fenves, Chun-Hao Chen, Henry Ho, and Eric Fujisaki. July 2000. $26.00

PEER 2000/05 *Performance-Based Evaluation of Exterior Reinforced Concrete Building Joints for Seismic Excitation.* Chandra Clyde, Chris P. Pantelides, and Lawrence D. Reaveley. July 2000. $15.00

PEER 2000/04 *An Evaluation of Seismic Energy Demand: An Attenuation Approach.* Chung-Che Chou and Chia-Ming Uang. July 1999. $20.00

PEER 2000/03 *Framing Earthquake Retrofitting Decisions: The Case of Hillside Homes in Los Angeles.* Detlof von Winterfeldt, Nels Roselund, and Alicia Kitsuse. March 2000. $13.00

PEER 2000/01 *Further Studies on Seismic Interaction in Interconnected Electrical Substation Equipment.* Armen Der Kiureghian, Kee-Jeung Hong, and Jerome L. Sackman. November 1999. $20.00

PEER 1999/14 *Seismic Evaluation and Retrofit of 230-kV Porcelain Transformer Bushings*. Amir S. Gilani, Andrew S. Whittaker, Gregory L. Fenves, and Eric Fujisaki. December 1999. $26.00

PEER 1999/12 *Rehabilitation of Nonductile RC Frame Building Using Encasement Plates and Energy-Dissipating Devices.* Mehrdad Sasani, Vitelmo V. Bertero, James C. Anderson. December 1999. $26.00

PEER 1999/11 *Performance Evaluation Database for Concrete Bridge Components and Systems under Simulated Seismic Loads.* Yael D. Hose and Frieder Seible. November 1999. $20.00

PEER 1999/10 *U.S.-Japan Workshop on Performance-Based Earthquake Engineering Methodology for Reinforced Concrete Building Structures.* December 1999. $33.00

PEER 1999/09 *Performance Improvement of Long Period Building Structures Subjected to Severe Pulse-Type Ground Motions*. James C. Anderson, Vitelmo V. Bertero, and Raul Bertero. October 1999. $26.00

PEER 1999/08 *Envelopes for Seismic Response Vectors.* Charles Menun and Armen Der Kiureghian. July 1999. $26.00

PEER 1999/07 *Documentation of Strengths and Weaknesses of Current Computer Analysis Methods for Seismic Performance of Reinforced Concrete Members.* William F. Cofer. November 1999. $15.00

PEER 1999/06 *Rocking Response and Overturning of Anchored Equipment under Seismic Excitations.* Nicos Makris and Jian Zhang. November 1999. $15.00

PEER 1999/05 *Seismic Evaluation of 550 kV Porcelain Transformer Bushings.* Amir S. Gilani, Andrew S. Whittaker, Gregory L. Fenves, and Eric Fujisaki. October 1999. $15.00

PEER 1999/04 *Adoption and Enforcement of Earthquake Risk-Reduction Measures.* Peter J. May, Raymond J. Burby, T. Jens Feeley, and Robert Wood. $15.00

PEER 1999/03 *Task 3 Characterization of Site Response General Site Categories*. Adrian Rodriguez-Marek, Jonathan D. Bray, and Norman Abrahamson. February 1999. $20.00

PEER 1999/02 *Capacity-Demand-Diagram Methods for Estimating Seismic Deformation of Inelastic Structures: SDF Systems*. Anil K. Chopra and Rakesh Goel. April 1999. $15.00

PEER 1999/01 *Interaction in Interconnected Electrical Substation Equipment Subjected to Earthquake Ground Motions*. Armen Der Kiureghian, Jerome L. Sackman, and Kee-Jeung Hong. February 1999. $20.00

PEER 1998/08 *Behavior and Failure Analysis of a Multiple-Frame Highway Bridge in the 1994 Northridge Earthquake.* Gregory L. Fenves and Michael Ellery. December 1998. $20.00

PEER 1998/07 *Empirical Evaluation of Inertial Soil-Structure Interaction Effects.* Jonathan P. Stewart, Raymond B. Seed, and Gregory L. Fenves. November 1998. $26.00

PEER 1998/06 *Effect of Damping Mechanisms on the Response of Seismic Isolated Structures.* Nicos Makris and Shih-Po Chang. November 1998. $15.00

PEER 1998/05 *Rocking Response and Overturning of Equipment under Horizontal Pulse-Type Motions.* Nicos Makris and Yiannis Roussos. October 1998. $15.00

PEER 1998/04 *Pacific Earthquake Engineering Research Invitational Workshop Proceedings, May 14–15, 1998: Defining the Links between Planning, Policy Analysis, Economics and Earthquake Engineering.* Mary Comerio and Peter Gordon. September 1998. $15.00

PEER 1998/03 *Repair/Upgrade Procedures for Welded Beam to Column Connections.* James C. Anderson and Xiaojing Duan. May 1998. $33.00

PEER 1998/02 *Seismic Evaluation of 196 kV Porcelain Transformer Bushings.* Amir S. Gilani, Juan W. Chavez, Gregory L. Fenves, and Andrew S. Whittaker. May 1998. $20.00

PEER 1998/01 *Seismic Performance of Well-Confined Concrete Bridge Columns.* Dawn E. Lehman and Jack P. Moehle. December 2000. $33.00